ELECTROCHEMICAL PATTERNING

ELECTROCHEMICAL PATTERNING OF TANTALUM AND TANTALUM OXIDE THIN FILMS

By

Hany El-Sayed, B.Sc.

A Thesis

Submitted to the School of Graduate Studies

in Partial Fulfillment of the Requirements

for the Degree

Master of Science

McMaster University

MASTER OF SCIENCE (2006) McMaster University

(Chemistry) Hamilton, Ontario

TITLE: Electrochemical patterning of tantalum and tantalum oxide thin films

AUTHOR: Hany ElSayed

SUPERVISOR: Dr. Peter Kruse

NUMBER OF PAGES: xi, 98

THESIS ABSTRACT

Nanoscale patterning research is motivated by two objectives: (i) tool development and (ii) scientific opportunities at small length scales. The first objective focuses on designing techniques that can be used to fabricate features as small as possible. Synthetic strategies of nanomaterials can be classified into two categories; bottom-up and top-down. The top-down approach involves reducing the size of a bulk material into nanoscale patterns, while the bottom-up approach refers to the build up of a material from the bottom, i.e. particle-by-particle. This particle maybe an atom, a molecule or even a cluster. In this work, two different top-down approaches were applied to create patterns in the nanoscale.

Direct selective metal deposition on semiconductors is of interest to electronic device technology, in particular for interconnects and Schottky devices. In this study, we investigated selective Cu electrodeposition on patterned tantalum oxide thin films. Cyclic voltammetry studies showed that tantalum oxide thin films of thicknesses higher than a certain critical value have insulating properties while oxide films of thicknesses less than this value are semiconductors. For the purpose of this study, tantalum oxide patterns of different thicknesses were created by electrochemical oxidation. Based on the aforementioned behavior of insulating and semiconducting tantalum oxide films, Cu lines were selectively electrodeposited on the tantalum oxide thin films patterns forming Schottky junctions. The process demonstrated in this work is compatible to standard

processes for semiconductor device fabrication while permitting flexible prototyping for research at the nanoscale.

The second method used to pattern nanoscale features on tantalum lead to the discovery of the first highly ordered nanoporous metal (template) prepared by electrochemical oxidation. The nanoporous tantalum has pores not only of high regularity and high diameter monodispersity, but also of tunable diameters in the range 27-55 nm. The template that has the highest hardness among other porous templates can be used for nanoparticles fabrication. The compatibility of the new porous tantalum template with semiconductor industry makes it a candidate for many potential technological applications.

STATEMENT OF STUDENT'S CONTRIBUTION

All the experimental work reported in this thesis "Electrochemical patterning of tantalum and tantalum oxide thin films" was done by Hany ElSayed except for the Nuclear Reaction Analysis (NRA) in chapters 2 and 3 which was partially done by Mark Greiner. The analysis of AFM data in chapters 3 and 4 was performed by Sherdeep Singh. All drafts and the final version of the thesis were written in their entirety by Hany ElSayed, with feedback from his supervisor.

ACKNOWLEDGEMENTS

This thesis (*Electrochemical patterning of tantalum and tantalum oxide thin films*) would not have evolved to its present form without the guidance and encouragement I have received from my colleague and friend, Dr. Peter Kruse. Under Dr. Kruse's enthusiastic, patient, and unequivocal supervision, I have learned how to take the right approach to solve problems that might arise. I have also learned a lot about surface chemistry, and that physical chemistry can be fun.

I cherish my friends within McMaster University's Department of Chemistry, from whom I received support and encouragement throughout my studies. Kevin, Guoxiu, Sung-Kyun, Sherdeep, Mark, and Subir – I will always remember joyfully enduring the blustery winter and sweltering summer seasons, both in-and-outside of the lab. I also thank from the staff Mrs. Carol Dada for her kind advice, and attentiveness.

Lastly, I want to thank, and dedicate this thesis to, my parents, Abd El-Wahab and Olfat, my wife, Rabaa, and my son AbduAllah. My family was really very patient and they gave me the real support most of the time and I am glad to let them know that I finally did it!

TABLE OF CONTENTS

Page

LIST OF FIGURES

Page

LIST OF TABLES

Page

CHAPTER 1

Introduction

1.1 Tantalum oxide thin films

Tantalum like most metals, is unstable when in contact with oxygen at room temperature, and, thermodynamically, should tend to form oxide. Despite its instability, (in the thermodynamic sense) tantalum finds use for the protection of equipment the survival of which in very corrosive environments must be assured[1]. The reason that tantalum works as a corrosion resistant material is that its reaction with air oxygen is limited by the formation of a thin but complete film of tantalum oxide that is insoluble in all solutions except hydrofluoric acid. The formed film separates the reactants, oxygen and tantalum, and further reaction can not occur unless by diffusion or migration (field-enhanced movement) of metal or oxygen ions through the film. These processes are usually very slow to occur on its own to form thick layers of tantalum oxide.

Tantalum oxide films are polycrystalline and their properties depend mainly on the stoichiometry, microstructure (grain size distribution), film thickness[2] and homogeneity[3]. The method by which tantalum is grown or deposited affects the aforementioned properties. Ta_2O_5 has been deposited or grown by many techniques such as radio frequency reactive sputtering[4], thermal oxidation[5], chemical vapor deposition (CVD)[6], plasma CVD[7], metalorganic chemical vapor deposition[8], ion assisted deposition[9], and anodization[3, 10-13].

Growing Ta_2O_5 films by anodization means oxidizing tantalum in an electrochemical cell containing either an aqueous or nonaqueous solution (wet anodization)[2, 10-16]. When a tantalum substrate covered with native oxide is placed in an electrolytic cell (with a solution that does not dissolve the oxide) as an anode, the applied potential creates an electrostatic field in the oxide, and this, as with many other metals, facilitates a continuous growth of the oxide film by causing tantalum or oxygen ions to be pulled into the film and move through it to react simultaneously at the two interfaces; tantalum/tantalum pentoxide and tantalum pentoxide/solution.

Anodic films are usually made either at constant current (galvanostatic), constant voltage (potentiostatic), or by a sequence of constant current and constant voltage. During the formation at constant voltage, the current falls continuously until leakage current predominates[1]. On the other hand, when a constant current is applied, the oxide film grows causing the potential difference across the two interfaces metal/oxide and oxide solution to increase until it reaches a steady value. In either techniques, it was found that when a defined current density and/or potential is applied, a linear relationship between the charge passed and the oxide thickness is obtained[2].

When the constant current technique is used to grow tantalum oxide films, equation (1) can be used to correlate the applied current density to the corresponding potential[17].

$$i = D \exp B\frac{V}{h} \qquad (1)$$

where i is the current density, V is the potential across the oxide film of thickness *h*, D and B are constants whose values depend on the electrochemical conditions and mainly the electrolyte composition and concentration.

Equation (2) is used to estimate the change in tantalum oxide thickness[2] (Δd) when a constant voltage is applied to tantalum substrate in 0.1 M H_2SO_4.

$$\Delta d = \frac{qV_m}{zF} \qquad (2)$$

where Δd is the change in oxide thickness ($=d - d_o$), q is the charge passed during anodic oxidation, V_m is the molar volume, z is the number of electrons in the overall reaction, and F is Faraday's constant. The change in oxide thickness is calculated relative to the initial thickness of the native oxide film thickness d_o because it is not possible to keep an oxide-free surface in aqueous solution. The molar volume of a compound can be determined as follows:

$$V_{Mi} = \frac{M_i}{\rho_i}$$

Where M_i and ρ_i are the molecular weight and density of compound (i), respectively.

Other formulas that relate quantity of charge passed to the oxide thickness grown in other electrolytes have been also used[18]. Different electrolyte solutions have been used to grow tantalum oxide films such as citric, oxalic, acetic, formic tartaric, phosphoric, and sulfuric acids[17].

Tantalum oxide when grown on a tantalum substrate may have semiconducting or insulating character depending on the oxide thickness. It was found that it behaves like a

semiconductor if it's thicknesses is less than ~15 nm, and like an insulators when it is thicker than this value[2]. XPS studies have shown that tantalum oxide films grown electrochemically are composed of two oxide layers; Ta_2O_5 and TaO_x. The TaO_x is a very thin oxygen deficient layer sandwiched between Ta and Ta_2O_5. The TaO_x thin oxygen deficient layer acts as n-type region and is an electron donor that is very effective if the oxide film is as thin as the native oxide(1-2nm)[19]. The charge carriers density decreases when the thickness of the film increases[18]. The basic electrical properties of anodically grown tantalum oxide thin and thick films were investigated by measuring the current-voltage (I-V) and capacitance-voltage (C-V) of the dry system Ta/tantalum oxide/metal.

In chapter 2 of the thesis, electrical properties of tantalum oxide thin films (thickness < 20 nm) were investigated by studying the cyclic voltammetry of the system tantalum/tantalum oxide/copper. In this chapter, tantalum oxide thin films were grown anodically and the thickness was estimated and experimentally measured by nuclear reaction analysis (NRA). The films have shown the anticipated behavior of being semiconductors or insulators depending on the thickness. Based on this unique behavior, patterned tantalum oxide substrate was prepared and selectively electroplated with copper.

1.2 Tantalum polishing

Tantalum polishing techniques can be categorized into three main divisions; mechanical polishing, chemical polishing, and electropolishing. Chemical polishing can be defined as a method in which substrate is immersed in a chemical solution that has the ability to homogeneously etch the substrate surface[20]. Chemical polishing is easy to do, fast, and does not require elaborate equipment. It usually performed in a beaker placed onto a magnetic stirrer. The substrate is hung in the solution or held with tongs. In case no stirring is required, the substrate can be placed at the bottom of the beaker and be brought up side down from time to time to make sure all the sides are polished. In some cases, chemical polishing is preceded by mechanical polishing to reduce the time required for chemical polishing. Most chemical etching solutions contain chemical compounds such as nitric acid, hydrofluoric acid, phosphoric acid and hydrogen peroxide. The disadvantage of this method is that a given volume of the solution can only polish a limited number of samples.

Tantalum is known to be resistant to all mineral acids except HF, thus most chemical etching solutions for tantalum contain HF and must be handled with great care[20]. It was found that addition of nitric acid accelerates the attack, thus the majority of etchants for tantalum contain HF and HNO_3 acids. Mixtures containing hydrofluoric acid and nitric acid and other chemical additives are unstable in air and they should be freshly prepared when used and discarded about one hour after mixing.

The following are examples of etchents used for tantalum:

i- 50% nitric acid, 50% hydrofluoric acid (48%)[21]

ii- HCl & HF (2:1)[20]

iii- Acetic acid & sulfuric acid & HF (2:5:1)[20]

Electropolishing is a process in which a metallic surface is smoothed by anodic dissolution in an adequate electrolytic solution[22]. In this method the substrate is usually polished mechanically first with SiC or other abrasives to a 600-grit, or equivalent, finish. The sample is then placed in a solution as an anode in an electrochemical cell. When the right combination of solution composition and concentration, solution temperature, applied potential, current density, and anodizing time is used, a smoothed and brightened surface is obtained.

The polishing conditions for a certain substrate-electrolyte combination can be evaluated by plotting the relationship between applied potential and the corresponding current density in a potentiodynamic experiment. Figure 1.1 shows a typical V-i curve of a potentiodynamic experiment for a polishing system[20].

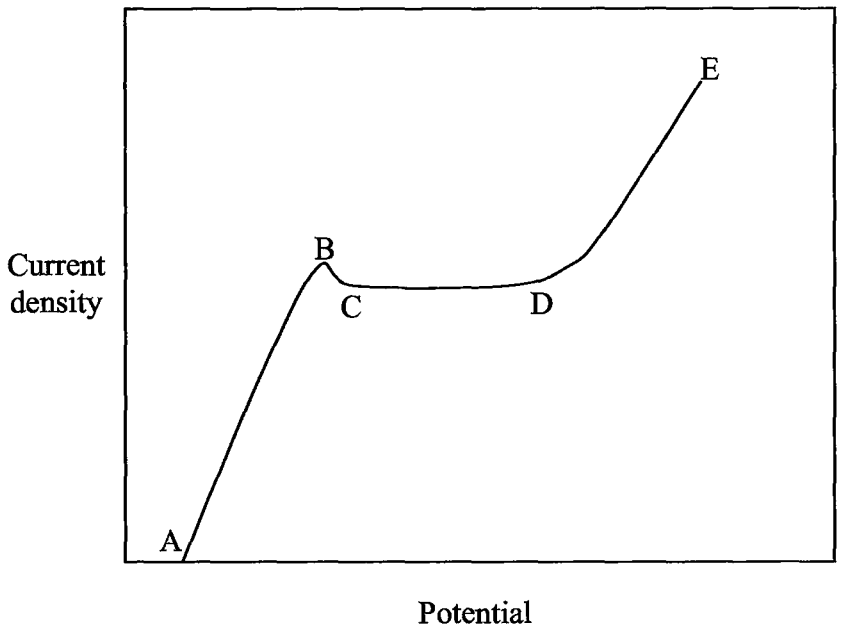

Figure 1.1 Potential-current density curve for a typical polishing system

Etching occurs at region (A-B), polishing occurs at region (C-D), and gas evolution and pitting occur at region (D-E). The anodic dissolution during electropolishing in region (C-D) is generally mass transport limited[22]. The theories that explain the limiting current plateau are based on either the salt film or the acceptor mechanism.

In the salt film mechanism, it is supposed that at region (C-D), i.e., at the mass controlled limiting current region, precipitation of a salt film occurs during anodic metal dissolution when the surface concentration of the salt exceeds its solubility[23]. Thus, the rate of the reaction depends on the dissolution of metal ions from that salt film away from the surface. In the acceptor mechanism, diffusion limited transport of an acceptor necessary for solvation is assumed, the acceptor being water or a complexing agent[22].

Electropolishing of tantalum is carried out in fluoride or perchlorate containing acidic solutions[22]. In this process, tantalum is connected to an electrochemical cell as an anode allowing it to grow passive oxide. The presence of aggressive ions in the polishing solutions and a relatively low water content facilitate the attack of the formed oxide that dissolves by pitting[22]. A higher content of water stabilizes the oxide chemically and thus prevents polishing.

The rate and mechanism in which passive tantalum oxide films dissolve depends on the electrochemical conditions in which they were allowed to grow. Electrochemical oxidation of tantalum in concentrate sulfuric or phosphoric acid solutions leads to the formation of anodic oxide films with remarkably different physical and chemical properties from those prepared in dilute solutions[13]. For instance, rates of dissolution in HF of the films formed in concentrated sulfuric or phosphoric acid solutions are much faster than those for the films grown in dilute solutions. The reason for this difference can be attributed to the incorporation of electrolyte anions into the oxide film. In a previous study, it was found that tantalum oxide films formed in 85% H_3PO_4 are consisted of a pure Ta_2O_5 layer and an outer PO_4^{3-} layer that represent 70 % of the whole oxide layer. On the other hand, when tantalum oxide is prepared in 95-98 % H_2SO_4, the whole film was found to have incorporated SO_4^{2-}.

In chapters 3 and 4, tantalum was electrochemically etched in concentrated sulfuric acid/HF solution. The resultant surface was a highly ordered porous surface that can be used as a template for nanoparticles fabrication. Some electrochemical conditions

that may affect the formation of pores such as anodization time, anodization potential, and aging were also studied.

1.3 References

1. Young, L., Anodic Oxide Films. *Section Title: Electrochemistry* **1961**, 377.
2. A. Radisic, G. O., P.C. Searson, Influence of oxide thickness on nucleation and growth of copper on tantalum. *Journal of the Electrochemical Society* **2004,** 151, C369-374.
3. Ezhilvalavan, S.; Tseng, T. Y., Preparation and properties of tantalum pentoxide (Ta_2O_5) thin films for ultra large scale integrated circuits (ULSIs) application - a review. *Journal of Materials Science: Materials in Electronics* **1999,** 10, (1), 9-31.
4. Nomura, K.; Ogawa, H.; Abe, A., Electrical-Properties of Al_2O_3-Ta_2O_5 Composite Dielectric Thin-Films Prepared by Rf Reactive Sputtering. *Journal of the Electrochemical Society* **1987,** 134, (4), 922-925.
5. Eftekhari, G., Mis Diodes on N-Inp with Tantalum Oxide Interfacial Layer Grown by Rapid Thermal-Oxidation of Tantalum. *Physica Status Solidi A-Applied Research* **1994,** 146, (2), 867-871.
6. Tabuchi, T.; Sawado, Y.; Uematsu, K.; Koshiba, S., Application of Penta-Di-Methyl-Amino-Tantalum to a Tantalum Source in Chemical Vapor-Deposition of Tantalum Oxide-Films. *Japanese Journal of Applied Physics Part 2-Letters* **1991,** 30, (11B), L1974-L1977.
7. Autran, J. L.; Paillet, P.; Leray, J. L.; Devine, R. A. B., Conduction properties of amorphous Ta_2O_5 films prepared by plasma enhanced chemical vapour deposition. *Sensors and Actuators A-Physical* **1995,** 51, (1), 5-8.

8. An, C. H.; Sugimoto, K., Ellipsometric Examination of Growth and Dissolution Rates of Ta_2O_5 Films Formed by Metalorganic Chemical Vapor-Deposition. *Journal of the Electrochemical Society* **1992,** 139, (7), 1956-1962.

9. Mcnally, J. J.; Aljumaily, G. A.; Mcneil, J. R., Ion-Assisted Deposition of Ta_2O_5 and Al_2O_3 Thin-Films. *Journal of Vacuum Science & Technology A-Vacuum Surfaces and Films* **1986,** 4, (3), 437-439.

10. Lu, Q.; Mato, S.; Skeldon, P.; Thompson, G. E.; Masheder, D.; Habazaki, H.; Shimizu, K., Anodic film growth on tantalum in dilute phosphoric acid solution at 20 and 85 degrees C. *Electrochimica Acta* **2002,** 47, (17), 2761-2767.

11. Shimizu, K.; Brown, G. M.; Habazaki, H.; Kobayashi, K.; Skeldon, P.; Thompson, G. E.; Wood, G. C., Direct observation of anodic films formed on tantalum in concentrated phosphoric and sulphuric acid solutions. *Corrosion Science* **1998,** 40, (6), 963-973.

12. Dell'Oca, C. J.; Young, L., Ellipsometric studies of anodic oxide films formed on tantalum in dilute phosphoric acid. *Section Title: Electrochemistry. Journal of the Electrochemical Society* **1970,** 117, (12), 1545-1548.

13. Vermilyea, D. A., Formation of anodic oxide films on tantalum in non-aqueous solutions. *Acta Met.* **1954,** 2, 483-486.

14. Amsel, G.; Cherki, C.; Feuillade, G.; Nadai, J. P., Influence of the electrolyte on the composition of 'anodic oxide films' on tantalum. *Journal of Physics and Chemistry of Solids* **1969,** 30, (9), 2117-2134.

15. Kerrec, O.; Devilliers, D.; Groult, H.; Marcus, P., Study of dry and electrogenerated Ta_2O_5 and $Ta/Ta_2O_5/Pt$ structures by XPS. *Materials Science & Engineering, B: Solid-State Materials for Advanced Technology* **1998,** B55, (1,2), 134-142.

16. Li, Y.-M.; Young, L., Non-Thickness-Limited Growth of Anodic Oxide Films on Tantalum. *Journal of the Electrochemical Society* **2001,** 148, (9), B337-B342.

17. Chaneliere, C.; Autran, J. L.; Devine, R. A. B.; Balland, B., Tantalum pentoxide Ta_2O_5 thin films for advanced dielectric applications. *Materials Science & Engineering R: Reports* **1998,** R22, (6), 269-322.

18. Kerrec, O.; Devilliers, D.; Groult, H.; Chemla, M., Dielectric properties of anodic oxide films on tantalum. *Electrochimica Acta* **1995,** 40, 719-724.

19. Shimizu, H.; Sugeno, F.; Nishimura, S.; Endo, H.; Honda, M., Electrical characterization of anodically oxidized Ta_2O_5 films. *Electrochemistry* **2004,** 72, (11), 737-742.

20. Voort, V., *Metallography Principles and Practice.* First ed.; McGraw-Hill, Inc. USA, 1984.

21. Hirsch, P. B.; al, e., Electron Microscopy of Thin Crystals. *Section Title: Electric Phenomena* **1977,** 563.

22. Piotrowski, O.; Madore, C.; Landolt, D., Electropolishing of tantalum in sulfuric acid-methanol electrolytes. *Electrochimica Acta* **1999,** 44, (19), 3389-3399.

23. Grimm, R. D.; West, A. C.; Landolt, D., Ac Impedance Study of Anodically Formed Salt Films on Iron in Chloride Solution. *Journal of the Electrochemical Society* **1992,** 139, (6), 1622-1629.

CHAPTER 2

Selective electroplating of copper lines on pre-patterned tantalum oxide thin films

H. ElSayed, M. Greiner and P. Kruse

2.1 Abstract

Direct selective metal deposition on semiconductors is of interest to electronic device technology, in particular for interconnects and Schottky devices. In this study, we investigate selective metal electrodeposition on patterned tantalum oxide thin films. Cyclic voltammetry studies show that tantalum oxide thin films of thicknesses higher than a certain critical value have insulating properties while oxide films of thicknesses less than this value are semiconductors. Copper thin films deposited on tantalum oxide films are known to form Schottky contacts. For the purpose of this study, tantalum oxide patterns of different thicknesses were created in three steps: a tantalum oxide film (insulator) was grown electrochemically, the film was then mechanically scratched to tantalum, the scratching was followed by mild oxidation to produce a tantalum oxide thin film. Based on the aforementioned behavior of insulating and semiconducting tantalum oxide films, metal lines were selectively electrodeposited on the tantalum oxide thin films patterns forming Schottky junctions. The process demonstrated in this paper is compatible to standard processes for semiconductor device fabrication while permitting flexible prototyping for research at the nanoscale.

2.2 Introduction

Electrochemical deposition of metals from solution is a cheap and easy-to-perform technique when compared to other metal deposition techniques such as chemical or physical vapor deposition in UHV[1]. Electrodeposition has several important advantages, e.g. it works at ambient pressure and temperature, it produces high quality deposits with excellent via/trench filling capabilities[2], it allows to deposit metals that are difficult to evaporate, and it can be used to plate metals onto substrates of complex geometries.

The interest in electrodeposition of metals onto semiconductors, especially on silicon surfaces, comes from its importance as a technique for the formation of Schottky barriers and Ohmic contacts in the fabrication of integrated circuits[1]. Metal deposition studies on silicon surfaces have been focused on the initial stages of nucleation and growth, including the deposition of Cu, Ag, Au, Co, and Ni on Si(100) and the deposition of Pb, Pt, Cd, and Cu on Si(111)[3].

The success in replacing aluminum metallization by copper in silicon device technology[4] has led to a renewal of interest in electrochemical deposition of metallic patterns onto silicon as well as onto various barrier materials such as tantalum, tantalum nitride, and tantalum oxide[5]. In order to create patterns of metals on silicon or barrier materials substrates, parallel nanofabrication approaches, such as photolithography and nanoimprint lithography, and lithographic techniques such as e-beam lithography (EBL) or focused ion-beam (FIB) are used. Although the last two technique have low throughput, they offer more flexibility when used for prototyping in a research environment.

EBL and FIB techniques in conjunction with locally introduced chemistry allow controlled patterning of deposited structures in deep-submicron dimensions[6]. EBL is considered a masking approach in which photoresists are provided that are resistant to deposition or etching environments[5]. FIB can be used directly to deposit metals on substrates, for instance, FIB has been recently used to directly deposit Pt to form low resistance metal contacts on n-type GaN[7]. It also can be used with the masking approach to deposit materials that can not be directly deposited on substrates.

In addition to masking approaches, several attempts have been made to employ direct patterning processes. An interesting electrochemical deposition approach is based on native differences in substrate activity, for instance, cobalt was selectively electrodeposited on pre-patterned p-/n- doped GaAs[8]. The semiconductor/ electrolyte interface forms a Schottky junction, the forward or reverse bias direction of which depends on the doping polarity. During the electrochemical deposition process, the semiconductor substrate serves as cathode and therefore is negatively polarized against the plating solution. Under these conditions, only n-GaAs was electroplated while p-GaAs worked as insulator. Atomic force microscopy (AFM) was also used to make scratches through a thin silicon oxide layer on a Si substrate. Due to the insulating nature of SiO_2, it worked as a mask in the electrodeposition process allowing copper plating to take place selectively in the scratched openings on silicon[9]. One drawback of the latter method is the direct deposition of copper on silicon.

Current copper metallization technology involves deposition of a diffusion barrier layer on top of silicon before copper deposition. The diffusion barrier, typically Ta, TaN, or TiN prevents copper metallization lines from diffusion into SiO_2 under high temperature conditions. Recently, ultrathin tantalum oxide (Ta_2O_5) films deposited by atomic layer deposition (ALD) were investigated as diffusion barrier[10]. The barrier thickness is predicted to decrease from 12 nm in the 100 nm node (year 2003) to only 2.5 nm in the 22 node by the year 2016. The studied oxide barriers within the thickness range of 1-4 nm deposited on silicon substrates were shown to be capable of preventing the diffusion of copper when they are covered with an approximately 100-nm-thick copper layer.

What makes tantalum oxide thin films interesting for nano-patterning is the unique behavior of being n-type semiconducting for thicknesses less than 15 nm, and insulating for thicknesses beyond 15 nm[11]. They are known to form a Schottky junction when a Au, Ag or Cu film is deposited on them[12].

In this study, we made use of these properties to report the selective electroplating of copper on pre-patterned tantalum oxide thin films grown anodically. The process of patterning involves creating a relatively thick, insulating tantalum oxide film (>20 nm) on a tantalum substrate by electrochemical oxidation. The oxide film is then scratched to expose the tantalum substrate underneath. A controlled mild electrochemical oxidation of the substrate results in a fresh oxide film (~4-5 nm) on the tantalum exposed by scratching. The pre-patterned substrate now has two different oxide film thicknesses (semiconducting and insulating) and can be subjected to copper electroplating. This

process allows copper to be electrodeposited selectively on the thinner oxide forming a Schottky contact. A high quality Schottky interface between the copper lines and the substrate is beneficial to applications such as four probe measurements of nanoscale objects (e. g. carbon nanotubes), where conduction through the bulk must be excluded.

In figure 2.1 we show a schematic diagram of the protocol used for the selective electrodeposition. In this method tantalum oxide film of at least 30 nm thickness was grown by anodic oxidation of tantalum substrate in 0.1 M H_2SO_4. The film was then scratched with a tungsten tip making linear scratches that expose tantalum underneath. The substrate was subjected to mild electrochemical oxidation to grow a tantalum oxide layer of about 4-5 nm thickness on the tantalum exposed by scratching. When the sample was electroplated in sulfate/EDTA solution, copper ions were selectively electrodeposited on the areas where the tantalum oxide layer is only 4-5 nm thick, i.e. in the openings made by scratching. The protocol that enabled making copper lines that form a Schottky junction with the substrate may find potential applications in the research and application of nanoscale devices due to its compatibility with processes currently used in the semiconductor industry.

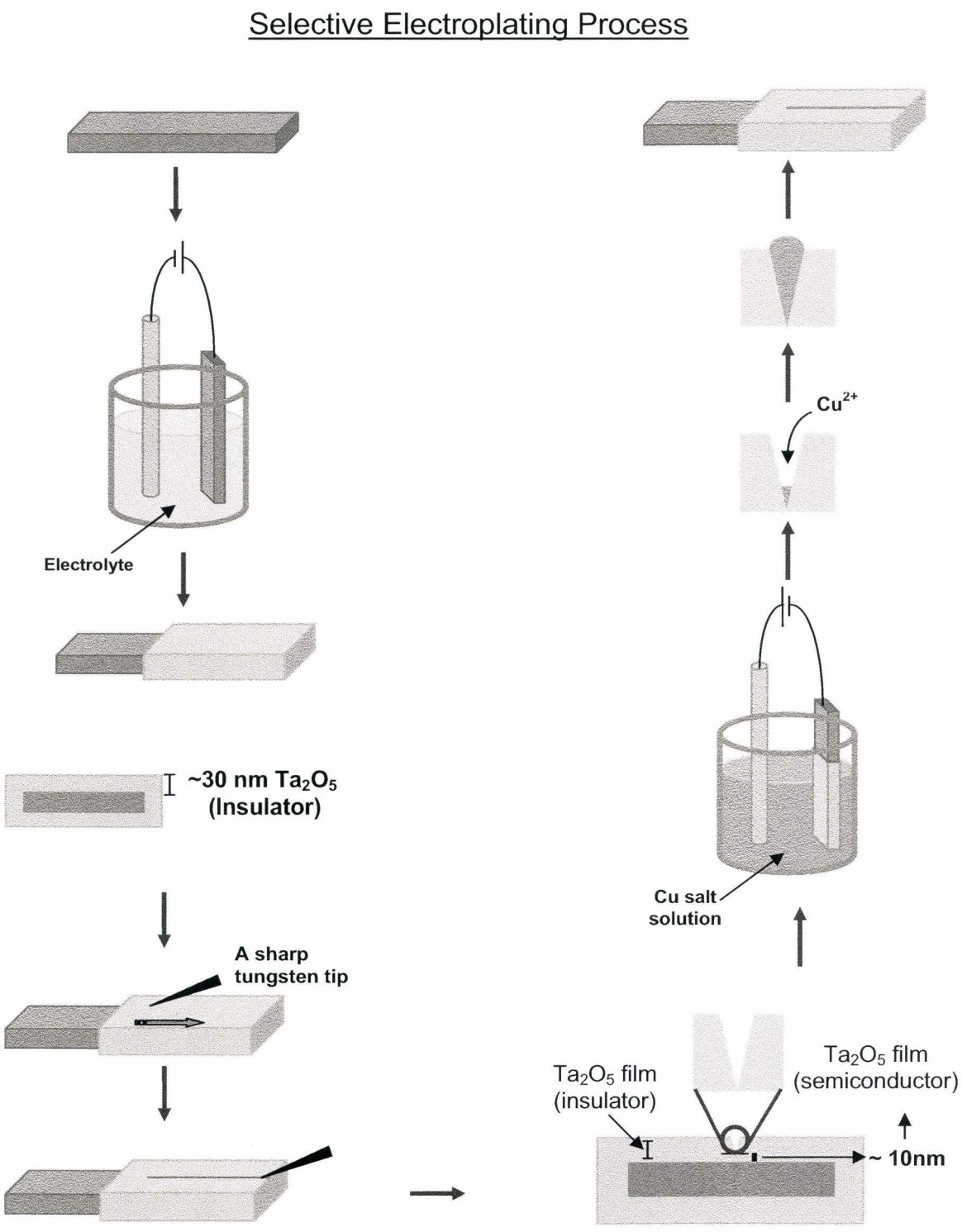

Figure 2.1. A schematic diagram of the protocol used for selective electrodeposition. Three main steps were involved: Ta_2O_5 oxide film formation, patterning (scratching), and electrodeposition.

2.3 Experimental work

Materials and surface preparation

Prior to anodic oxidation or electrodeposition, tantalum foil (Alfaaesar, 99.95%, 0.127 mm) was rinsed in acetone, isopropanol, and Millipore water (18.2 MΩ/cm resistivity). Oxide was grown by anodization in 0.1 M H_2SO_4. For the electrodeposition study, three solutions were used, copper sulfate, cupper sulfate PEG, cupper sulfate EDTA. The copper sulfate solution contained 0.05 M $CuSO_4.5H_2O$ and 0.375 M H_2SO_4. The copper sulfate PEG solution (pH 0.25) contained 0.05 M $CuSO_4.5H2O$, 0.375 M H_2SO_4, 1.82 x 10^{-5} M polyethylene glycol (PEG) (average M_n 3400) and 3.03 x 10^{-4} M Cl^- as KCl. The copper sulfate EDTA solution was 0.05 M $CuSO_4.5H_2O$ and 0.1 M EDTA with the pH adjusted to 13.5 using NaOH[13]. The solutions were prepared from reagent-grade chemicals and Millipore water (18.2 MΩ/cm resistivity). Tungsten wires (purity 99.9+%, Aldrich, USA) were used as tip material for tantalum oxide scratching. NaOH (purity 97.0%, AlfaAesar) pellets were used as received to prepare a 3 N solution for tips electrochemical etching.

Electrochemical experiments

Anodization was conducted using a conventional three-electrode system connected to a potentiostat (Autolab PGSTAT30). Tantalum oxide films were grown in 0.1 M H_2SO_4 at constant potential with a Pt/Ir wire as a counter electrode, calomel reference electrode (0.241 V vs. SHE), and tantalum as a working electrode. At each potential, growth was terminated when current reached steady state (i.e. dI/dt relatively

constant). The electrochemical experiments (Cyclic voltammetry (CV) and chronoamperometry) were performed in a three electrode glass cell with a calomel reference electrode positioned close to the working electrode, and a Pt/Ir wire as a counter electrode. All potentials were reported vs. the calomel electrode.

Electrochemical etching of tungsten wires

Oxide film scratching was done by an electrochemically etched tungsten tip. Extremely Sharp tips with low aspect ratio were prepared by etching 0.25 mm W wire in NaOH solution (3N). The STM tips were electrochemically etched using the "loop" technique as previously reported in the literature[14]. A drop of the etching solution (3 N NaOH) was placed on a platinum/iridium wire ring cathode so as to produce a thin film. The wire was then placed through this film and a potential applied between the ring electrode and the wire. Etching was complete in a few minutes. The lower part of the wire fell away from the ring and was carefully collected in a small Teflon tube, shorter than the length of the lower tip so that the side walls did not touch the tip apex.

Scanning electron microscopy (SEM) and Energy Dispersive X-ray (EDX) surface investigations

Images of the anodized samples were acquired on a field emission scanning electron microscope (FE-SEM Jeol 7000F). The elemental composition of surface features after copper deposition on the tantalum oxide substrates was determined using a Jeol energy-dispersive X-ray (EDX) spectrometer installed on a field emission scanning

electron microscope (FE-SEM Jeol 7000F). Both scanning electron microscopes were employed to observe the surface morphology of the deposits as well. The initial beam energy used in the EDX was 20 KeV and that for the scanning electron microscopy (SEM) analyses was 20 or 15 kV.

Nuclear reaction analysis (NRA) measurements

The $^{16}O(d,p)^{17}O$ nuclear reaction was used to determine the absolute oxygen content of the anodized samples within ~0.5 μm of the surface. The $^{16}O(d,p)^{17}O$ reaction used an 972 KeV deuterium beam as the primary beam. The set-up used is located at the Van-de-Graaff lab at Interface Science Western, University of Western Ontario. The incident beam is approximately 1mm in diameter. The ion beam was incident on the samples along the surface normal and the detector was placed at 125° in the scattering plane which included the incident beam. The tantalum oxide thickness was estimated by comparing the number of protons emitted from the sample to those emitted from a reference Ta_2O_5 sample of known oxygen coverage and oxide thickness using the $^{16}O(D, p)^{17}O$ reaction. The accuracy of this measurement is about ±5% if the sample and reference have similar geometry. More about the experimental setup of the NRA system can be found elsewhere[15].

2.4 Results and discussion

Growth and characterization of oxide films:

Ta_2O_5 films of different thicknesses were grown by electrochemical oxidation at constant potentials of 2, 4, 6, 8, and 10 V in 0.1 M H_2SO_4 . Compact tantalum pentoxide films are formed by the electrochemical oxidation of tantalum according to reaction (1)[16, 17], with the obtained oxide thickness depending on the applied potential.

$$2Ta + 5\,H_2O \longrightarrow Ta_2O_5 + 10H^+ + 10e^- \quad (1)$$

XPS analysis has shown[18] that a "native oxide layer", composed of 12 mol% of TaO and 88 mol% of Ta_2O_5, is already present at the surface of tantalum. In addition, "electrogenerated oxides" are composed of 97mol% of Ta_2O_5, and only 3 mol% of TaO. Therefore, it may be considered that Ta_2O_5 is the main component of the electrogenerated oxide. The current efficiency for reaction (1) is essentially 1 because the rates of side reactions such as oxygen evolution are negligible[11]. Hence the thickness of the electrogenerated oxide (Δd) can be determined from

$$\Delta d = \frac{qV_m}{zF}$$

where Δd is the change in oxide thickness ($=d - d_o$), q is the charge passed during anodic oxidation, V_m is the molar volume, z is the number of electrons in the overall reaction, and F is Faraday's constant. The change in oxide thickness is calculated relative to the

initial thickness of the native oxide film thickness d_o because it is not possible to keep an oxide-free surface in an aqueous solution[11].

The molar volume of a compound can be determined as follows:

$$V_{Mi} = \frac{M_i}{\rho_i}$$

Where M_i and ρ_i are the molecular weight and density of compound (i), respectively.

Figure 2.2 shows the change in film thickness vs. anodic oxidation potential. The change in film thickness was determined from the charge passed during oxidation, using $V_m = 50.6\ cm^3\ mol^{-1}$ and $z = 10$.

A linear variation of the oxide film thickness with respect to the applied potential was observed. The slope of the line calculated by linear regression is 1.45 nm V^{-1}. This linear relationship is valid for the whole thickness range and allowed us to estimate the thickness of all electro-generated tantalum oxide layers. The fluctuation in the experimental conditions such as temperature, electrolyte composition and concentration affect the reaction kinetics and in turn change the reaction yield. This is probably the reason of getting a different value for the slope obtained in this study than those given by other authors: 1.76nmV^{-1} [19], 1.67nmV^{-1} [18] and 1.57 nm V^{-1} [20].

Nuclear reaction analysis (NRA) was used to verify absolute thicknesses of our tantalum oxide films because it is an established technique for quantitative analysis of the oxygen content within ~0.5 μm of the surface. The *absolute* tantalum oxide thickness of anodized samples was estimated by comparing the number of protons emitted from the

sample to those emitted from a reference Ta_2O_5 sample of known oxygen coverage and oxide thickness using the $^{16}O(D, p)^{17}O$ reaction[21].

The use of the NRA technique in this study to provide accurate estimate of the oxide thickness grown electrochemically assumes that the oxide layer is relatively flat and of uniform composition (97mol% of Ta_2O_5). Some representative NRA spectra, including that from the Ta_2O_5 standard, are shown in figure 2.3. The absolute oxide thickness of the sample was calculated by comparing area under peak $^{16}O(d,p_1)^{17}O$ to that of the standard. By subtracting the native tantalum oxide thickness (1.5 nm)[19] from all the *absolute* oxide thicknesses of all samples measured by NRA, the *change* in film thickness vs. anodic oxidation potential can be obtained (Figure 2.2).

It is very clear from figure 2.2 that thickness values measured by NRA are higher than those estimated by charge calculation. It is known that tantalum oxide anodically grown in concentrated acids has different chemical and physical properties than that grown in dilute acids[22]. Tantalum oxide grown in concentrated sulfuric acid (95-98%) is characterized by electrolyte anion (SO_4^{2-}) incorporation in the whole depth of the film[15]. The overestimation of oxide thickness results from the excess oxygen incorporated in the oxide as sulphate ions.

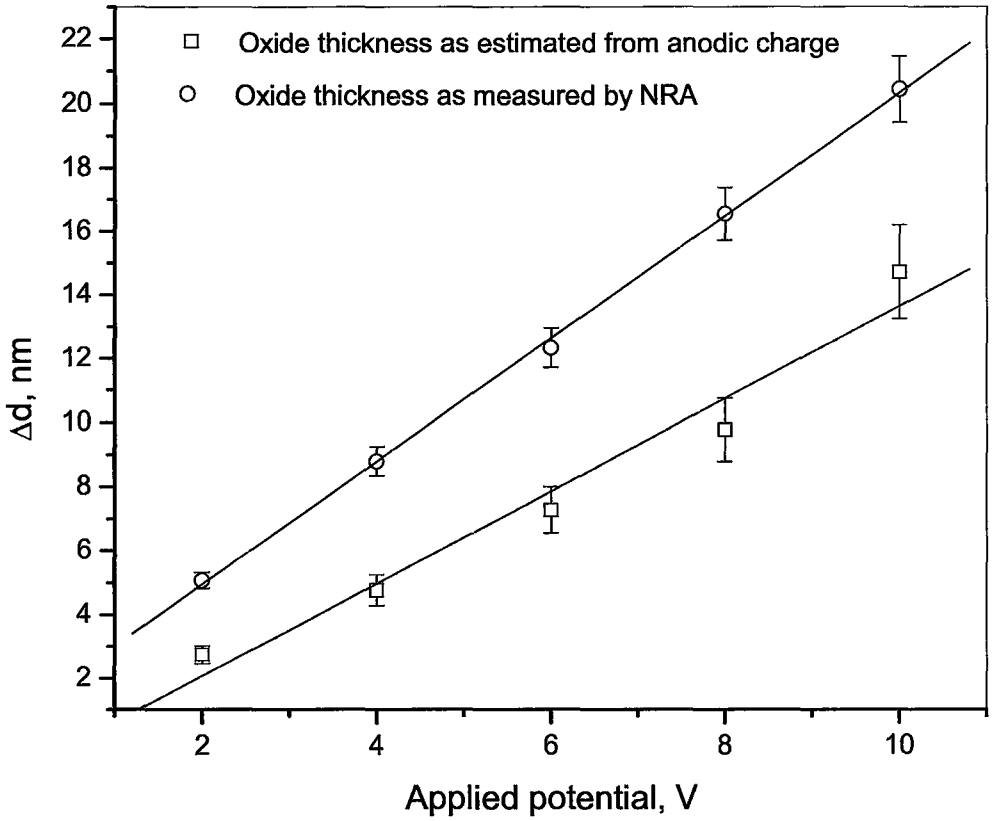

Figure 2.2. Change in oxide thickness (Δd) (▫) as estimated from anodic charge calculations, and (o) as calculated from NRA vs. anodic oxidation potential. Tantalum foil was anodized at constant potentials; 1, 2, 4, 6, 8, and 10 V in 0.1 m H_2SO_4. Potential was measured vs. standard calomel electrode (0.241 V vs. SHE).

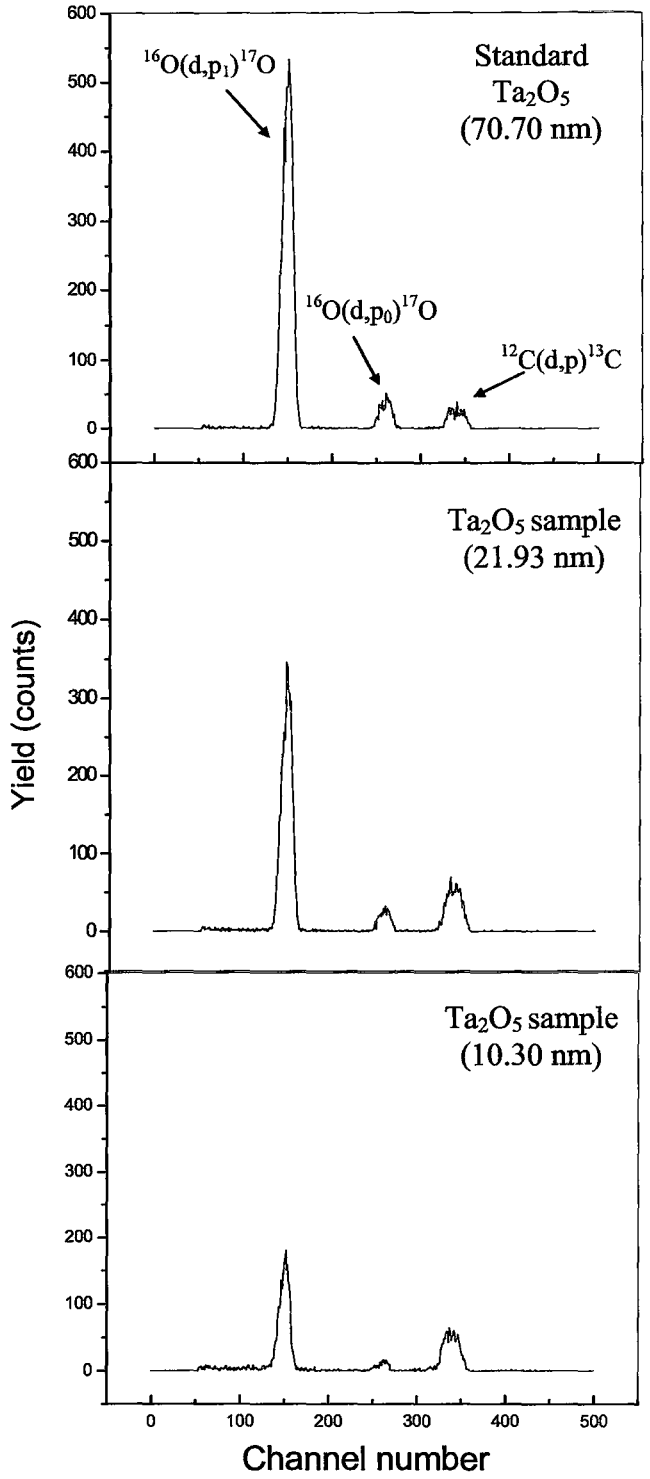

Figure 2.3. NRA spectra obtained for the following targets: (a) Ta_2O_5 calibrated standard (70.7 nm); (b) Electrochemically grown Ta_2O_5 (21.93nm); and (c) Electrochemically grown Ta_2O_5 (10.30 nm).

Copper electrodeposition on tantalum oxide:

Figure 2.4(a) shows the cyclic voltammogram for a native oxide film on tantalum in 50 mM $CuSO_4.5H_2O$ and 375 mM H_2SO_4, collected at 10 mV s^{-1} between 0.8 V and -0.8 V. In the forward scan (0.8 V to -0.8 V), the onset of copper deposition occurs at about -0.4 V and is followed by a characteristic peak associated with nucleation and diffusion-limited growth at about -0.72 V[11]. In the reverse scan (-0.8 V to 0.8 V), copper deposition continues up to 0.04 V, 0.76 V positive to the cathodic peak potential, indicating a very large nucleation overpotential. A small peak of 0.12 mA/cm^2 which represents copper stripping is observed at 0.14 V.

The large cathodic peak in combination with a very small stripping peak indicates the irreversible nature of copper electrodeposition on native tantalum oxide. This behavior is known as "diode-effect" or "Schottky behavior" that causes the resistance against anodic reactions (such as copper stripping in this case) to be much larger than the resistance against cathodic reactions[23] (such as copper ions reduction in this work).

The cyclic voltammograms obtained for the anodically grown tantalum oxide thin films (6.5 nm and 11.5 nm thick) in 50 mM $CuSO_4.5H_2O$ and 375 mM H_2SO_4 are shown in figure 2.4(b). The two CVs are characterized by a copper deposition peak that is shifted to more positive potential than that obtained on native oxide, and a decrease in the peak intensity as the oxide thickness increases. On the reverse scan, no stripping peaks were observed at all. This suggests that copper deposition on tantalum oxide thin films grown electrochemically was irreversible (diode-like behavior).

The observed Schottky behavior can be explained based on the electronic structure of tantalum oxide films. Thin tantalum oxide films consists of two layers, Ta_2O_5 and TaO_x. The TaO_x is a very thin oxygen deficient layer sandwiched between Ta and Ta_2O_5. The TaO_x thin oxygen deficient layer acts as n-type region and is an electron donor that is very effective if the oxide film is as thin as the native oxide(1-2nm)[19]. The doping effect starts to fade as the thickness of tantalum oxide increases and becomes negligible beyond ~15 nm oxide thickness, making tantalum oxide films thicker than 15 nm insulating. This explains why a small stripping peak was obtained with native oxide and no anodic peaks were observed with electrochemically grown tantalum oxide. In the later case the films are thick enough to allow cathodic currents but not anodic currents.

It is a remarkable feature of all three voltammograms that they all show a cross over between the anodic and cathodic part. Such a "crossed" voltammogram is not an usual feature of direct deposition, but is indeed expected in the presence of 3-D nucleation[23]. Our findings agree with a previous study[12] that investigated the current-voltage (*I-V*) characteristics of a dry M(Au, Ag, or Cu)/Ta_2O_5/Ta system and showed that a Schottky barrier could have been formed at the Au, Ag, or Cu/ Ta_2O_5 interface.

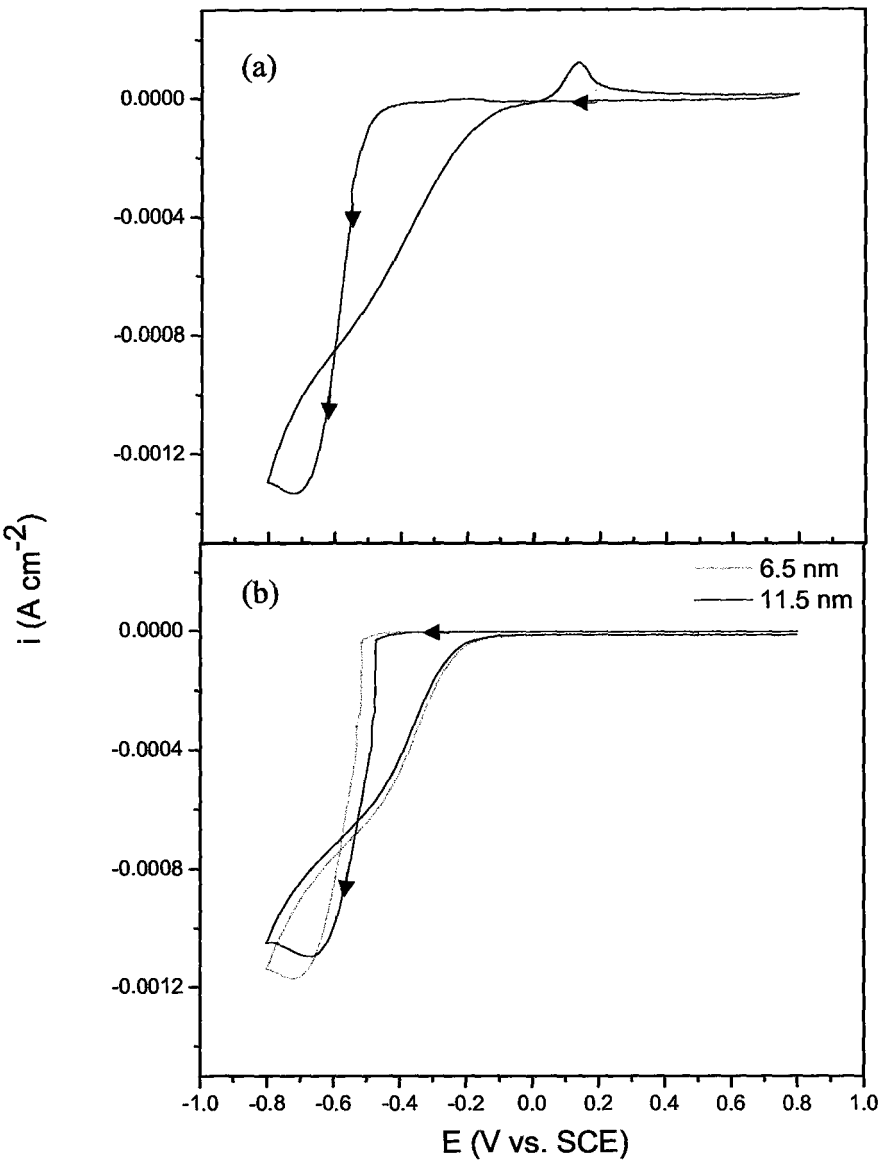

Figure 2.4. Cyclic voltammograms for electrodeposition of copper from 50 mM $CuSO_4.5H_2O$ and 375 mM H_2SO_4, collected at 10 mV s^{-1} on (a) native tantalum oxide film, and (b) anodically grown tantalum oxide thin films (6.5 and 11.5 nm thick).

The reproducibility and stability of the Schottky junction formed at the Ta_2O_5/Cu interface was examined by repeating each CV for 20 times. Figure 2.5(a) shows 20 CVs for tantalum (native oxide) in copper sulfate/sulfuric solution. It is very clear from the graph that Schottky interface is stable and reproducible. The cathodic peak shifts to less negative potential with number of cycles indicating increasing amount of deposited copper on substrate surface. This shift is very obvious in the first 10 cycles, where the cathodic peak of the first cycle appears at -0.721 mV, and that of the tenth cycles appears at -0.401 mV. The shift is not significant during the last ten cycles where the cathodic peak of the eleventh cycle appears at -0.396 mV and that of the twentieth cycle appears at -0.371 mV. Figure 2.6 shows cathodic peak position (potential) with respect to cycle number.

Figure 2.5 (b) and 2.5 (c) show the 20 CVs of tantalum oxide thin films of 6.5 nm and 11.5 nm thickness, respectively, in copper sulfate/sulfuric acid bath. Cathodic peaks show the same potential shift behavior observed in figure 2.5 (a) in addition to the absence of stripping peaks indicating improvement of the Schottky junction performance. Figure 2.5 (d) shows the CV of tantalum oxide thin film of ~ 20 nm thickness in copper sulfate/sulfuric solution. The CV does not show any cathodic or anodic peaks indicating the insulating nature of the oxide film.

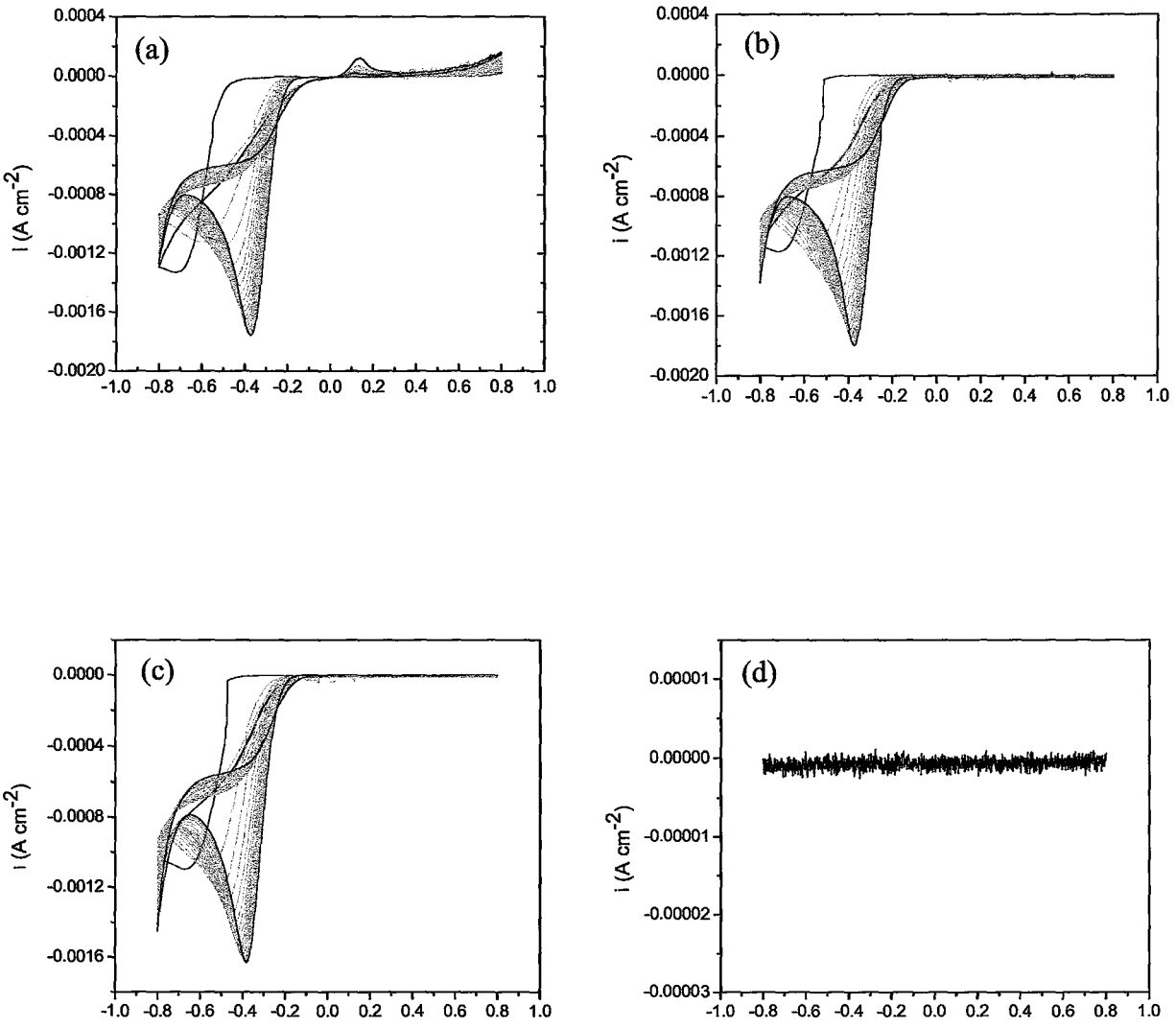

Figure 2.5. 20 CVs for electrodeposition of copper from 50mM $CuSO_4.5H_2O$ and 375mM H_2SO_4, collected at 10 mV s^{-1} on (a) native tantalum oxide film, (b) anodically grown tantalum oxide thin film (6.5 nm thick), (c) anodically grown tantalum oxide thin film (11.5 nm thick), and (d) anodically grown tantalum oxide thin film (~20 nm thick).

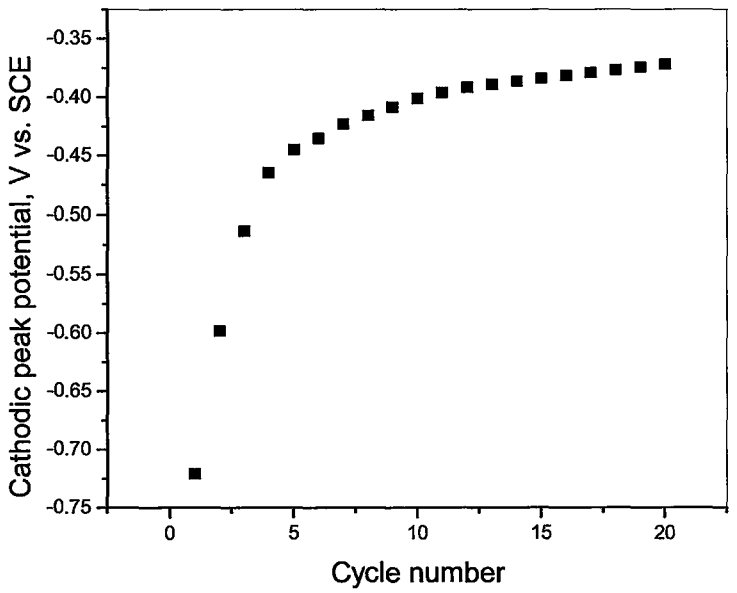

Figure 2.6. Cathodic peak position (V vs. SCE) with respect to cycle number. Potential values of cathodic peaks and corresponding cycle numbers are obtained from Figure 8 (a).

Effect of organic additives on copper electrodeposition kinetics and copper deposits morphology:

Copper plating baths containing organic additives are used in copper metallization technology. The successful void-free filling, or "super-filling," of trenches with electrodeposited copper has been achieved in an acidic plating bath containing several bath additives[24] such as polyethylene glycol (PEG), chloride ions and EDTA. In general, these organic additives are known to enhance the rate of deposition at the bottom of features such as trenches or vias, leading to void-free deposits[25].

Figure 2.7 shows cyclic voltammograms for native tantalum oxide in copper sulfate/PEG (pH 0.25) and copper sulfate/EDTA (pH 13.5) solutions. In both baths, the cyclic voltammograms for depositing copper on native tantalum oxide are similar to those obtained for copper deposition on TaN but significantly different from those obtained for depositing copper from similar baths on Pt[25]. The copper deposition onset potential is shifted more negative than that previously reported for copper on Pt: by ~ 0.6 V for the case of sulfate/PEG and ~ 0.5 V for sulfate/EDTA. The shift in the deposition peak may be attributed to the large nucleation overpotential on native tantalum oxide. No copper deposition peak is observed in the cathodic direction because it is overlapped with the hydrogen evolution peak in the CVs of the two examined solutions. This behavior indicates that the copper clusters catalyze the hydrogen evolution reaction.

For the voltammogram of native tantalum oxide in sulfate/PEG bath, current fluctuations in the reverse scan were detected. Such a behavior has been reported before

for the CVs obtained by depositing copper on TaN and it was found that these fluctuations are associated with the appearance of cracks in the deposited films[25]. In sulfate/PEG solution, the copper deposition current becomes zero at about 0 V, several hundred milli- volts negative of the zero current potential on Pt[25]. In sulfate/EDTA solution, the voltammogram shows almost the same behavior as that of sulfate/PEG solution except for current fluctuations which were not detected in the reverse scan. The small stripping peaks observed in the reverse scan of the two examined solutions suggest the formation of a Schottky junction at the tantalum oxide/copper interface.

The deposition transients (i-t curves) of copper deposition on native tantalum oxide were analyzed to investigate the mechanism of nucleation and growth. In these experiments, the potential was stepped from a potential where no deposition is observed, typically the open circuit potential, to potentials in the region of the bulk deposition peak, as determined from the cyclic voltammograms. Figure 2.8 shows current transients for copper deposition from sulfate/PEG (a) and sulfate/EDTA (b) solutions on native tantalum oxide. The transients were characterized by a dramatic initial increase in current density due to nucleation and growth of three-dimensional (3D) copper clusters. At longer times the current increases slowly indicating the growth of copper nuclei but nucleation does not occur any more.

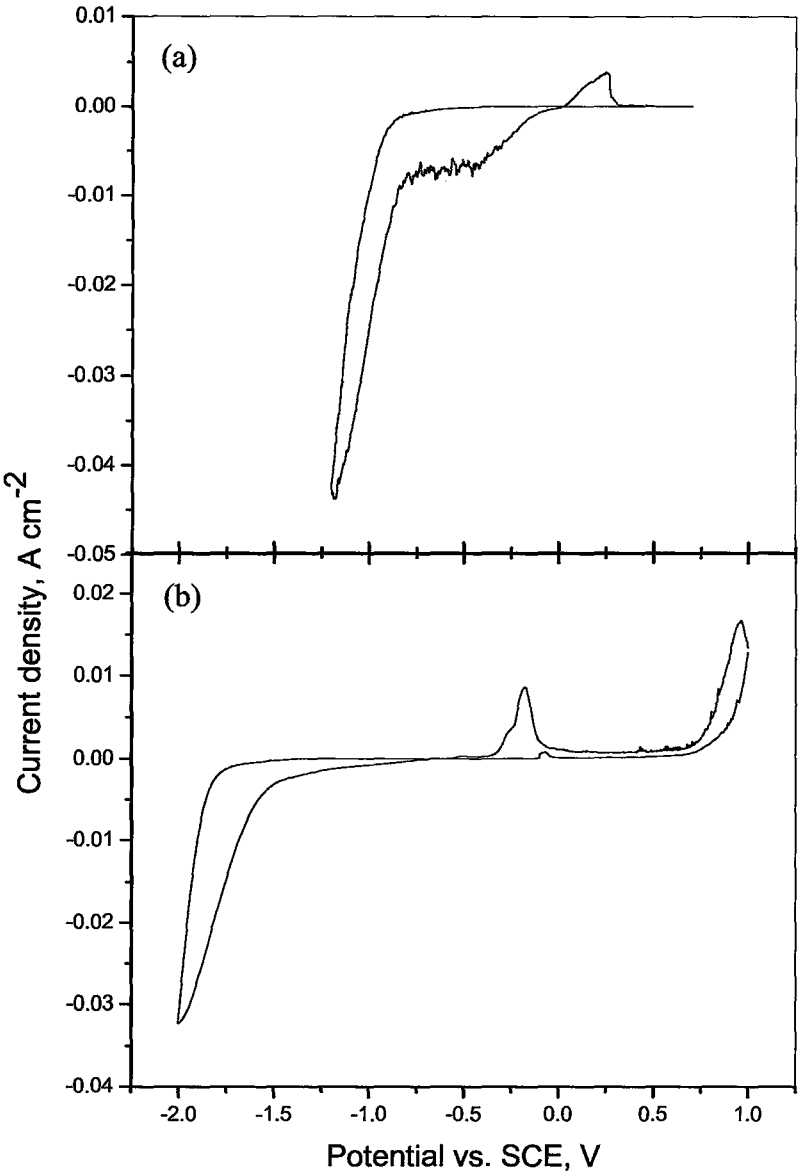

Figure 2.7. Cyclic voltammograms for electrodeposition of copper from (a) copper sulfate/PEG (pH 0.25), and (b) copper sulfate/EDTA (pH 13.5) solutions.

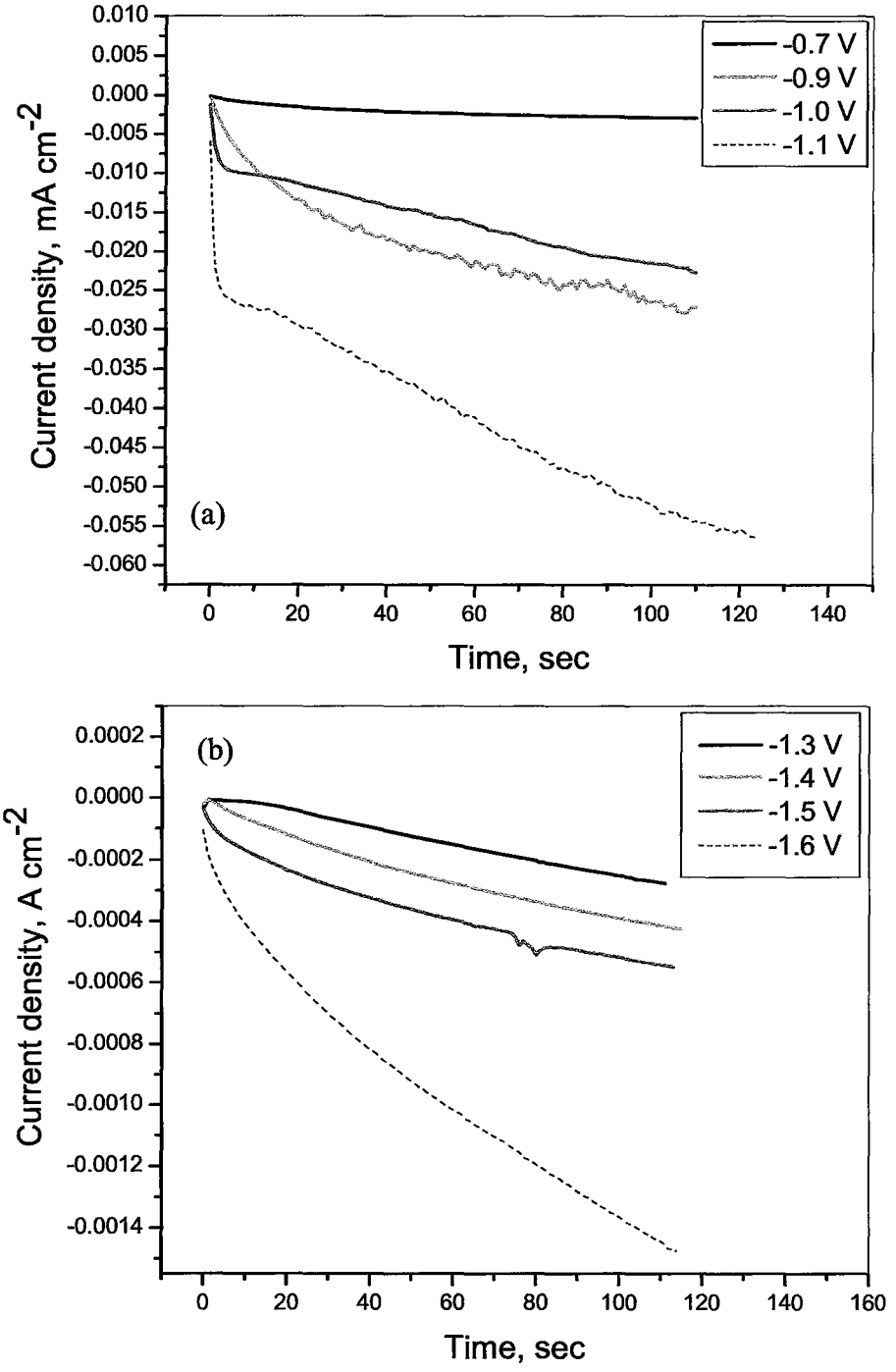

Figure 2.8. current transients curves for copper deposition from (a) sulfate/PEG, and (b) sulfate/EDTA solutions on native tantalum oxide.

Figure 2.9 shows a series of field emission scanning electron microscope (FE-SEM) images of copper clusters deposited at -0.9 V, -1.0 V, and -1.1 V from copper sulfate/PEG solution. All images were recorded after 110 seconds of electrodeposition under a fixed potential. For all potentials, the clusters were randomly distributed on the surface. The images show that the cluster density increases with increasing deposition potential but they do not form a copper film on the substrate. This increases the chances of forming discontinuous patterns when this bath is used for selective electroplating.

Copper deposition on native tantalum oxide from sulfate/EDTA solution was characterized by producing copper patches on the surface. An FE-SEM image of one of these copper patches is shown in figure 2.10(a). EDX analysis showed that the composition of the patch deposited from sulfate/EDTA bath is mainly copper with a significant percentage of potassium. The spectrum is shown in figure 2.10(b). The sulfate/EDTA solution contains KOH in order to bring the pH to 13.5, causing the potassium peak in the spectrum. The oxygen peak in the EDX spectrum is a result of copper oxidation and tantalum oxide.

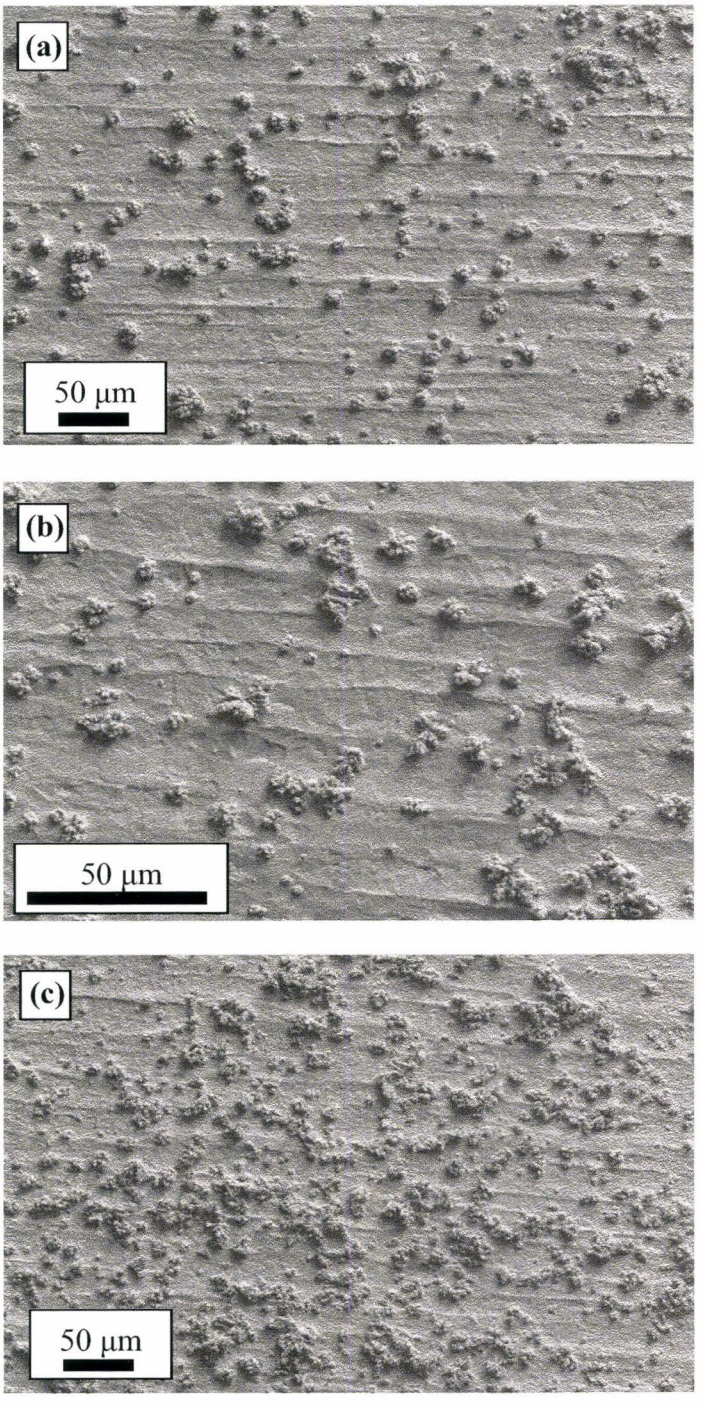

Figure 2.9. Series of plan view field emission scanning electron microscope (FE-SEM) images of copper clusters deposited at (a)-0.9, (b) -1.0, and (c) -1.1 V from copper sulfate/PEG solution. All images were recorded after 110 second of electrodeposition.

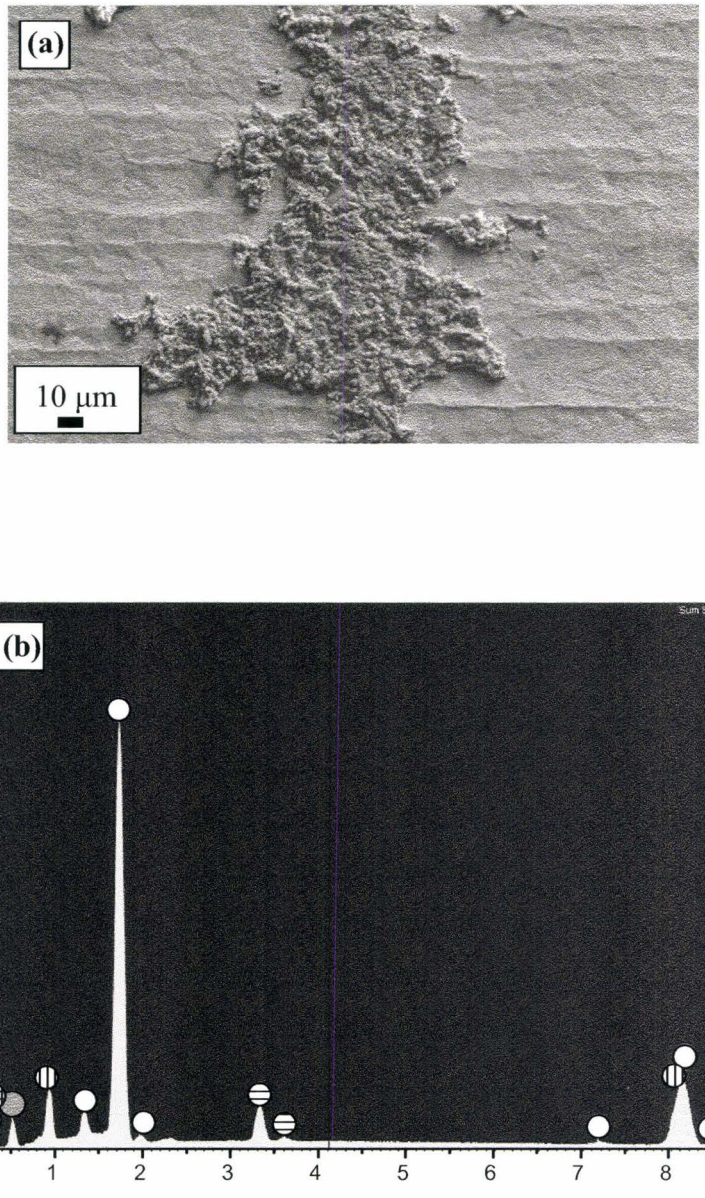

Figure 2.10. (a) An FE-SEM image of copper deposited from $CuSO_4$/EDTA solution at -1.5 V on native tantalum oxide. (b) EDX spectrum represents the whole area scanned in (a). Ta is represented on the spectrum as white circle, Cu as ⓓ , K as ⊖, O as ◍ , and C as ⊕.

Figures 2.11 (a, c) show FE-SEM images of copper clusters selectively electroplated from sulphate/EDTA solution on a pre-patterned tantalum oxide substrate. The images show that copper is only electrodeposited on the thinner tantalum oxide and no copper clusters were observed on the thicker oxide. Therefore the protocol of selective electrodeposition can work efficiently to form microstructures on pre-patterned tantalum oxide substrates. Figures 2.11 (b, d) show EDX copper maps of the FE-SEM images (a and c repectively). The EDX copper maps confirm the identity of the electrodeposited structure to be mainly copper. The discontinuity of copper lines is due to the relatively poor nucleation of copper on tantalum oxide[18].

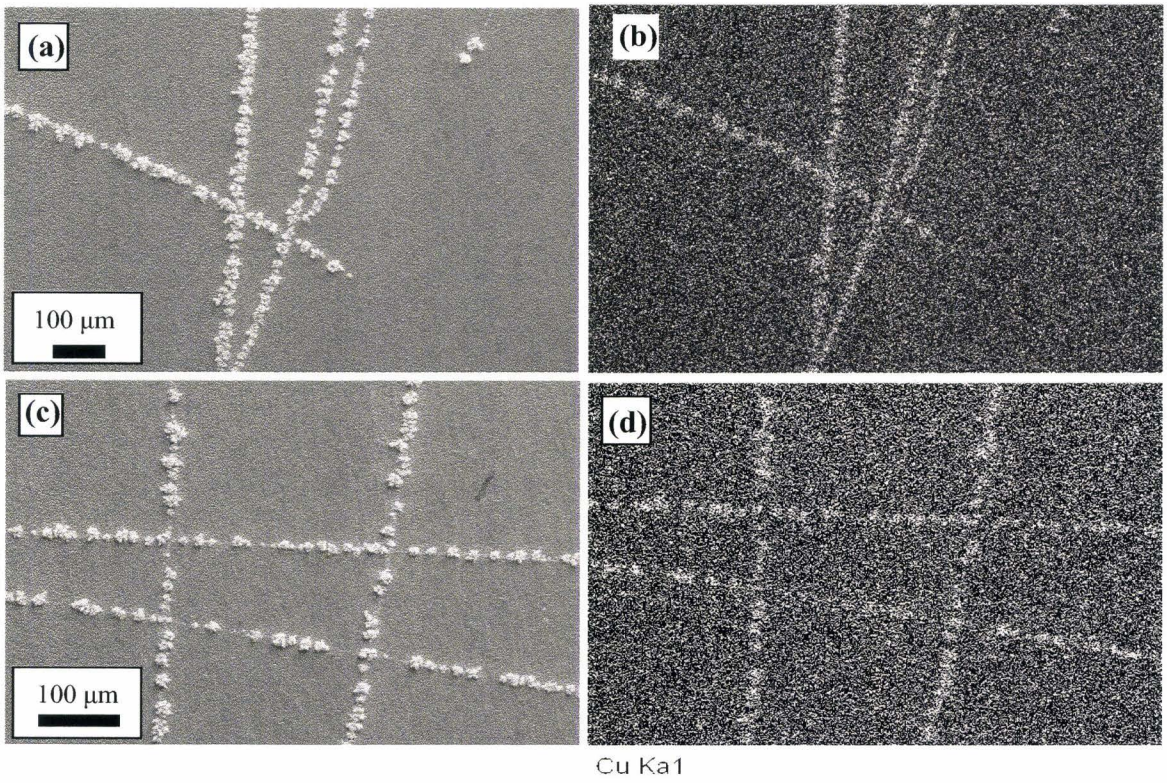

Figure 2.11. (a and c) FE-SEM images of copper clusters selectively electroplated on a pre-patterned tantalum oxide substrate. (b and d) The corresponding EDX copper map of FE-SEM images (a and c).

2.5 Conclusion

Our study has shown that metals, copper in this work, can be electroplated on pre-patterned tantalum oxide thin films of appropriate thickness. In the process of selective electrodeposition, a tantalum oxide thin film of 30 nm thick, insulating oxide acts as a mask while patterned oxide films ~4 nm thick, n-type semiconductor, were successfully copper electroplated. The electrodeposited copper does not re-dissolve because of the Schottky junction formed at the Ta_2O_5(< 15 nm thick)/Cu interface.

The rectifying behavior of the resulting Schottky junction was investigated by cyclic voltammetry for tantalum oxide films (thickness < 15 nm) in acidified copper sulfate solution. All the investigated systems showed cyclic voltammograms with either a very small anodic peak or no stripping peaks at all, along with large peaks for copper deposition (cathodic peaks). The ability to perform selective electrodeposition of metals on semiconductor substrate, such as Ta_2O_5(< 15 nm thick), could enable the maskless fabrication of semiconductor devices. It can be also used for prototyping by building four point probe for instance, that can be used for in-situ electrical measurements of nanoscale objects.

2.6 Acknowledgements

We acknowledge William N. Lennard (Interface Science Western) for his great assistance with the NRA analysis of our samples and Steve Koprich (Brockhouse Institute for Materials Research) for help with the SEM. We also thank Gillian Goward (McMaster) for helpful discussions. Financial support was provided by the Department of Chemistry at McMaster University and the National Science and Engineering Research Council of Canada. H. E. was supported by a post-graduate fellowship from the Ford Foundation (IFP program).

2.7 References

1. Ziegler, J. C.; Wielgosz, R. I.; Kolb, D. M., Pb deposition on n-Si(111) electrodes. *Electrochimica Acta* **1999,** 45, (4-5), 827-833.
2. Pasa, A. A.; Schwarzacher, W., Electrodeposition of thin films and multilayers on silicon. *Physica Status Solidi A-Applied Research* **1999,** 173, (1), 73-84.
3. Ji, C. X.; Oskam, G.; Searson, P. C., Electrodeposition of copper on silicon from sulfate solution. *Journal of the Electrochemical Society* **2001,** 148, (11), C746-C752.
4. Andricacos, P. C.; Uzoh, C.; Dukovic, J. O.; Horkans, J.; Deligianni, H., Damascene copper electroplating for chip interconnections. *IBM Journal of Research and Development* **1998,** 42, (5), 567-574.
5. Schmuki, P.; Erickson, L. E., Selective high-resolution electrodeposition on semiconductor defect patterns. *Physical Review Letters* **2000,** 85, (14), 2985-2988.
6. Gannon, T. J.; Gu, G.; Casey, J. D.; Huynh, C.; Bassom, N.; Antoniou, N., Focused ion beam induced deposition of low-resistivity copper material. *Journal of Vacuum Science & Technology B* **2004,** 22, (6), 3000-3003.
7. Nam, C. Y.; Kim, J. Y.; Fischer, J. E., Focused-ion-beam platinum nanopatterning for GaN nanowires: Ohmic contacts and patterned growth. *Applied Physics Letters* **2005,** 86, (19), 193112.

8. Scheck, C.; Evans, P.; Schad, R.; Zangari, G.; Sorba, L.; Biasiol, G.; Heun, S., Selective metal electrodeposition through doping modulation of semiconductor surfaces. *Applied Physics Letters* **2005,** 86, (13), 133108.

9. Santinacci, L.; Djenizian, T.; Schmuki, P., A semiconductor nano-patterning approach using AFM-scratching through oxide thin layers. *Materials Research Society Symposium Proceedings* **2002,** 740, (Nanomaterials for Structural Applications), 205-210.

10. Alen, P.; Vehkamaki, M.; Ritala, M.; Leskela, M., Diffusion barrier properties of atomic layer deposited ultrathin Ta_2O_5 and TiO_2 films. *Journal of the Electrochemical Society* **2006,** 153, (4), G304-G308.

11. A. Radisic, G. O., P.C. Searson, Influence of oxide thickness on nucleation and growth of copper on tantalum. *Journal of the Electrochemical Society* **2004,** 151, C369-374.

12. Shimizu, H.; Sugeno, F.; Nishimura, S.; Endo, H.; Honda, M., Electrical characterization of anodically oxidized Ta_2O_5 films. *Electrochemistry* **2004,** 72, (11), 737-742.

13. Moffat, T. P.; Bonevich, J. E.; Huber, W. H.; Stanishevsky, A.; Kelly, D. R.; Stafford, G. R.; Josell, D., Superconformal electrodeposition of copper in 500-90 nm features. *Journal of the Electrochemical Society* **2000,** 147, (12), 4524-4535.

14. Rao, M. V. H.; Mathur, B. K., Sharp Tungsten Tips for Scanning Tunneling Microscope Prepared by Electrochemical Etching Process. *Indian Journal of Pure & Applied Physics* **1993,** 31, (8), 574-576.

15. Shimizu, K.; Brown, G. M.; Habazaki, H.; Kobayashi, K.; Skeldon, P.; Thompson, G. E.; Wood, G. C., Direct observation of anodic films formed on tantalum in concentrated phosphoric and sulphuric acid solutions. *Corrosion Science* **1998,** 40, (6), 963-973.

16. Bispinck, H.; Ganschow, O.; Wiedmann, L.; Benninghoven, A., Combined SIMS, AES, and XPS investigations of tantalum oxide layers. *Applied Physics* **1979,** 18, (2), 113-117.

17. Young, L., *Anodic Oxide Films*. ed.; Academic Press Inc: 1961.

18. Kerrec, O.; Devilliers, D.; Groult, H.; Chemla, M., Dielectric properties of anodic oxide films on tantalum. *Electrochimica Acta* **1995,** 40, 719-724.

19. Macagno, V.; Schultze, J. W., The growth and properties of thin oxide layers on tantalum electrodes. *Journal of Electroanalytical Chemistry* **1984,** 180, (1-2), 157-170.

20. Montero, I.; Albella, J. M.; Duart, J. M. M., Reformation Processes of the MnO_2-Ta_2O_5-Ta System Under Galvanostatic Conditions. *Electrochimica Acta* **1990,** 35, (5), 855-859.

21. Amsel, G.; Cherki, C.; Feuillade, G.; Nadai, J. P., Influence of the electrolyte on the composition of 'anodic oxide films' on tantalum. *Journal of Physics and Chemistry of Solids* **1969,** 30, (9), 2117-2134.

22. Vermilyea, D. A., Formation of anodic oxide films on tantalum in non-aqueous solutions. *Section Title: Electrochemistry. Acta Met.* **1954,** 2, 483-486.

23. Emery, S. B.; Hubbley, J. L.; Roy, D., Voltammetric and amperometric analyses of electrochemical nucleation: Electrodeposition of copper on nickel and tantalum. *Journal of Electroanalytical Chemistry* **2004,** 568, 121-133.

24. Hasegawa, M.; Okinaka, Y.; Shacham-Diamand, Y.; Osaka, T., Void-free trench-filling by electroless copper deposition using the combination of accelerating and inhibiting additives. *Electrochemical and Solid State Letters* **2006,** 9, (8), C138-C140.

25. A. Radisic, Y. C., P. Taephaisitphongse, A.C. West, P.C. Searson, Direct copper electrodeposition on TaN barrier layers. *Journal of the Electrochemical Society* **2003,** 150, C362-C367.

CHAPTER 3

Highly ordered porous tantalum for nanofabrication, the first porous metal prepared by anodic oxidation

Hany ElSayed, Mark Greiner, Sherdeep Singh, and Peter Kruse

3.1 Abstract

Synthetic strategies of nanoparticles have been developed, ranging from chemical preparation methods to lithographic techniques. The later methods offer very high control over the position, shapes and dimensions of the nanoparticles, however they lack to the materials versatility, simplicity and cost-efficiency in nanofabrication. Template-assisted nanofabrication that entails the synthesis of the desired nanostructure inside the pores of the nanoporous material has demonstrated successful control over size and shape of nanostructures. In this paper we report the synthesis of the first metallic nanoporous template by electrochemical oxidation. The template that has not only pores of high regularity and monodispersity but also highest hardness among other porous templates may be used for nanoparticles fabrication. The compatibility of the new porous tantalum template with semiconductor industry makes it a candidate for many potential technological applications.

3.2 Introduction

The large interest in nanomaterials comes from their numerous potential applications in fields such as biomedical sciences, electronics, optics, magnetism, energy storage, materials and electrochemistry. Synthetic strategies of nanomaterials can be classified into two categories; bottom-up and top-down. The top-down approach involves reducing the size of a bulk material into nanoscale patterns, while the bottom-up approach refers to the build up of a material from the bottom, i.e. particle-by-particle. This particle maybe an atom, a molecule or even a cluster. Regardless the utilized approach, the main concern in fabricating nanostructures is the control of the final morphology of the product. This concern originates from the fact that nanostructures properties are size and/or shape dependent[1]. One of the bottom-up methods recently demonstrated successful control over size and shape of nanostructures is the template-assisted nanofabrication[2, 3]. This method entails the synthesis of the desired nanostructure inside the pores of the nanoporous membrane. The most common templates used for nanostructures fabrication are ion-track etched membranes[4] and porous alumina[5]. However, there are a variety of other porous materials that could be used as templates. The ion-track etched membranes are prepared by bombarding a nanoporous sheet with nuclear fission fragments to create damage tracks in the material, and then chemically etching these tracks into pores[2]. The result of this process is randomly distributed nanochannels of uniform diameter (as small as 10 nm). The other type of templates, porous alumina, is prepared by anodic oxidation of aluminum in acid solutions[6]. Nanochannels of uniform diameter are formed normal to the surface of aluminum as a result of the anodic oxidation process. The dimensions of

the channels can be tuned by controlling the electrochemical conditions such as anodizing time, applied potential and electrolyte composition and concentration. The cylindrical pores of porous alumina have been used to grow nanoparticles, nanowires and nanotubes. The question now arises whether other metals of technological interest can also be used to grow nanoporous films that can be used for nanostructures fabrication. To date, however, titanium[7], niobium[8], tungsten[9], Zirconium[10] and tantalum[11] have been anodically oxidized under electrochemical conditions where they form pores. When Ti is anodized in fluoride ion containing phosphate electrolytes, self-organized titanium oxide nanotubes are formed[7]. On the other hand irregular porous oxide films were obtained by anodic oxidation of niobium[8, 12, 13], and tungsten[9]. Recently, random porous tantalum oxide films with a wide pore size distribution were obtained by anodizing tantalum in dilute sulfuric acid solutions containing small quantities of HF (0.5-3%)[11, 14, 15].

It is known that tantalum can be anodized in almost any aqueous electrolyte except concentrated hydrofluoric to produce compact tantalum oxide[16]. During anodization the electrostatic field E in the pre-existing oxide film (native oxide) causes metal ions to enter the oxide and travel through the oxide to the electrolyte where they react to produce more oxide. Oxygen in the electrolyte also migrates through the oxide under the effect of the electrostatic field to the metal where more oxide is also produced.

Anodic oxidation of tantalum in concentrated acid solutions also leads to the growth of compact tantalum oxide films but these films have distinctly different physical and chemical properties from those formed in dilute solutions. Further, films formed in concentrated acid solutions show higher dissolution rates in HF than those formed in

dilute acid solutions[17]. These differences in the chemical and physical properties and dissolution rates arise from increased incorporation of electrolyte anions into the films formed into the concentrated solutions[18].

In this research paper we report, for the first time, the fabrication of a highly 2D ordered porous tantalum by simple electrochemical oxidation. The porous tantalum is characterized by high pore diameter monodispersity. The anodization was conducted in a mixture of concentrated sulfuric acid and dilute hydrofluoric acid. The porous tantalum can be used as a template for nanoparticles fabrication. The high degree of pore diameter monodispersity will be reflected upon the nanostructures prepared in the pores of the new template. Given that tantalum has the third highest melting point among metals, the porous tantalum template can be safely used for nanostructures synthesis with high temperature deposition techniques. The compatibility with present semiconductor technology and simplicity of preparation make the porous tantalum a universal, practical template not only for nanoparticles fabrication for the semiconductor industry but also for the field of nanostructuring in general.

3.3 Experimental work

Materials and surface preparation

Prior to anodization, tantalum foil (Alfaaesar, 99.95%, 0.127 mm) was rinsed in acetone, isopropanol, and Millipore water (18.2 MΩ/cm resistivity). No polishing process was adapted. Anodization was carried out in a stirred solution of concentrated H_2SO_4 (95-98%) and HF (48%) in a volume ratio 9:1. (This solution will be referred to below as "solution *A*.") The solutions were prepared from reagent-grade chemicals and Millipore water.

Electrochemical experiments

Anodization was conducted using a conventional two-electrode system connected to a power supply (Agilent E3615A). A Pt/Ir wire was used as the counter-electrode (cathode). The working electrode (anode) was tantalum foil substrate connected with a copper wire to the power supply. The distance between the working and counter-electrodes was kept at 1.5 cm. During anodization, solution was stirred using a magnetic bar. All the experiments were performed at room temperature (approximately 20°C). Immediately after anodization, the sample was rinsed with deionized water.

Scanning electron microscopy and Atomic force microscopy surface investigations

The surface view of the anodized samples were acquired on a field emission scanning electron microscope (FE-SEM Jeol 7000F). The AFM used is Digital Instruments Nanoscope III system, a Multimode SPM.

Nuclear reaction analysis (NRA) measurements

The $^{16}O(d,p)^{17}O$ nuclear reaction was used to determine the absolute oxygen content of the anodized samples within ~0.5 μm of the surface. The $^{16}O(d,p)^{17}O$ reaction used an 972 KeV deuterium beam as the primary beam. The incident beam is approximately $1mm^2$ in area. The ion beam was incident on the samples along the surface normal and the detector was placed at 125° in the scattering plane which included the incident beam. The tantalum oxide thickness was estimated by comparing the number of protons emitted from the sample to those emitted from a reference Ta_2O_5 sample of known oxygen coverage and oxide thickness using the $^{16}O(d, p)^{17}O$ reaction. The accuracy of this measurement is about ±5% if the sample and reference have similar geometry. More about the experimental setup of the NRA system can be found elsewhere[19].

3.4 Results and discussion

Morphology:

Figure 3.1(a) illustrates the surface view of the formed anodic porous tantalum by a field emission scanning electron microscope (FE-SEM). The anodization was conducted in "solution *A*" at 24°C at 20V for 15 minutes. The micrograph shows that in this specific sample the formed pores have an average diameter in the range 30-50 nm and they are symmetric and highly ordered.

In contrast to porous anodic alumina, the first self-ordered nano-channel material formed by anodization, in which defects and dislocations accumulate at the grain boundaries[20] and long range anodization is required to attain a defect-free porous surface, defects and dislocations in anodic porous tantalum do not concentrate at the grain boundaries between domains and the pores are oriented along the grain boundaries. Figure 3.1(b) shows an FE-SEM image of a tantalum sample anodized at the aforementioned H_2SO_4/HF solution at 12V for 20 minutes. In this image the pores are well organized even along the grain boundaries and they are highly monodisperse having pore diameter in the range 27-30 nm. The few defects and imperfections shown in image (1b) are randomly distributed and they do not concentrate at the grain boundaries.

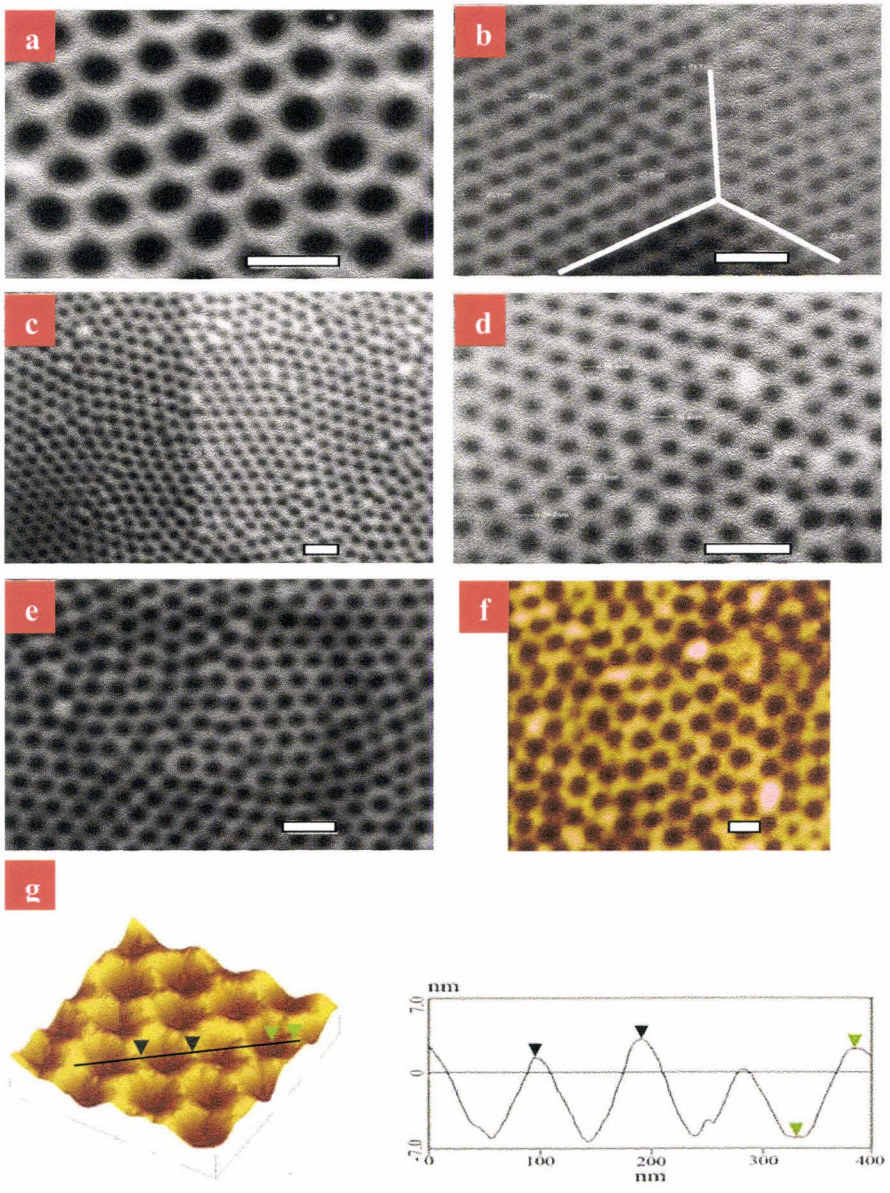

Figure 3.1. SEM images of porous tantalum. a, anodized for 15 min at 20V. **b**, anodized for 20 min at 12V. **c**, anodized for 10 min at 15V. **d**, anodized for 10 min at 12V. **e**, anodized for 10 min at 12V (two months old sample). **f**, **AFM of porous tantalum** anodized for 12 min at 15V, and **g**, 3D view AFM image and its corresponding cross section. (All the rod bars are 100 nm.)

Trying to find the optimum electrochemical conditions at which highly ordered porous tantalum of high monodisperse characters can be obtained, tantalum samples were anodized at different values of potential and anodizing time. It was observed that relatively short time anodization (5-60 min) at potentials in the range 10-20V produces highly ordered porous tantalum. Figure 3.1(c) shows an FE-SEM image of a tantalum sample after anodization in "solution *A*" at 15V for 10 minutes. In the shown FE-SEM image the pores look highly ordered and monodisperse in diameter, most of them have diameters in the range 35-37 nm. Image (1d) shows the surface view of a tantalum sample anodized for 10 minutes at 12 V. The pores show high order and monodisperse character. It is worth mentioning that porous tantalum was also obtained at very short time of anodizing, as short as 5 minutes.

The long term stability of the pores was studied by FE-SEM, where a sample was investigated once prepared and two month after preparation. Image 1(e) shows the plane view of a two months old porous tantalum sample. The pores did not show any kind of deformation after two month left in air and they still show the high monodisperse character.

To confirm our results, an atomic force microscope (AFM) was used in order to obtain real-space topographical images of the pores with nanometer resolution. The data obtained enabled us to determine the minimum pore depth, and the variation of the pore wall height. Non-contact mode AFM was used to avoid destruction of the pores. The images were obtained in ambient atmosphere using a Digital Instruments Nanoscope III system. Figure 3.1(f) shows an AFM image of porous tantalum anodized at 15 V for 12

min. The AFM image (1 μm x 1 μm) confirms the regular distribution of the pores on the surface. Figure 3.1(g) shows a 3D view of a smaller area (400 nm x 400 nm) of the scanned sample. A cross section of the 3D AFM image shows that the average pore wall to wall distance is ~90 nm and the average pore depth appears to be at least 10 nm.

The influence of anodizing potential on the pore diameter was investigated by using the optimized experimental conditions. The minimum and maximum observed pore diameter formed at each potential were drawn against the applied potential. Figure 3.2 shows pore diameter ranges of the obtained porous tantalum vs. the applied potential. The graph shows that there is a trend of pore diameter increase as the applied potential increases.

The effect of anodizing time on pore diameter of randomly distributed porous tantala grown in dilute sulfuric acid was studied by Schmoki et al group[11, 14]. They have shown that the average pore diameter and the thickness of the porous tantalum oxide increase with anodization time. In contrast to their findings, it was found that when concentrated sulfuric acid is used, no significant change in the pore diameter with anodization time was observed. The effect of anodizing time on oxide thickness was studied by nuclear reaction analysis (NRA).

NRA gives the total number of oxygen atoms in a given sample surface area and compare it to that of a flat tantalum oxide thin film of known thickness. Using NRA, it was found that the absolute thicknesses of tantalum oxide films on porous tantalum samples grown at different anodizing times are almost the same and the oxide thickness

does not depend on time of anodization. NRA measurements on the various porous tantalum samples are summarized in Table (1).

The measured oxide thickness values are in the range 3.0-3.7 nm, i.e. slightly thicker than native tantalum oxide thickness (1-2nm)[21, 22]. The measured values may be overestimated because of the incorporation of electrolyte anions into the oxide film during electrochemical oxidation. Tantalum oxide grown in concentrated sulfuric acid (95-98%) is characterized by electrolyte anion (SO_4^{2-}) incorporation in the whole depth of the film[18]. This is typically the case for tantalum oxide formed on top of porous tantalum. The overestimation of oxide thickness results from the excess oxygen incorporated in the oxide as sulphate ions.

The formation of porous tantalum rather than porous tantala in concentrated sulfuric acid can be explained by the chronoamperometric curves obtained while etching the tantalum.

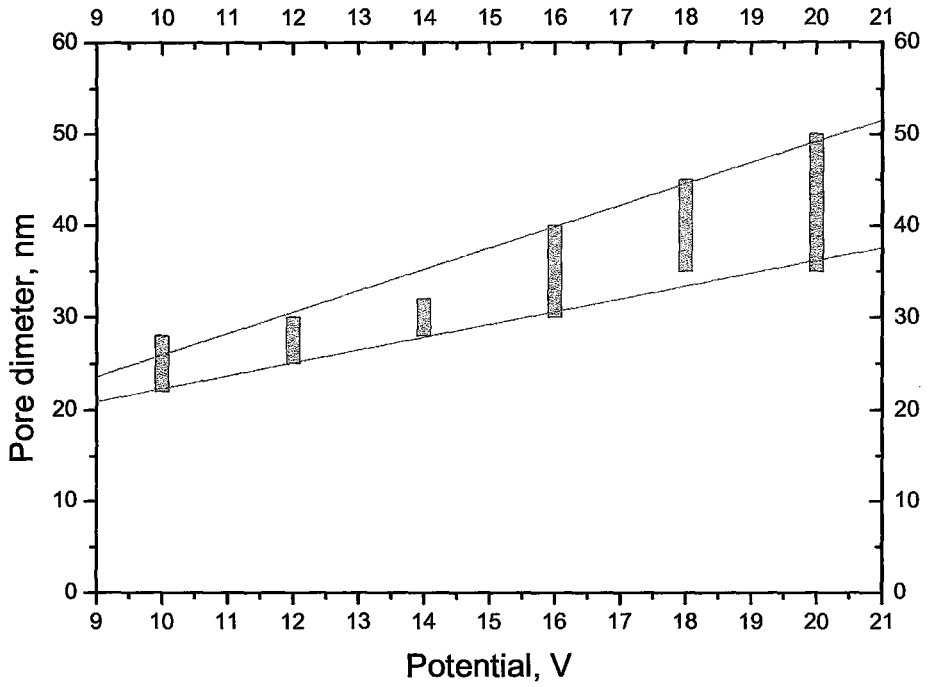

Figure 3.2. The minimum (lower end of the bar) and maximum (higher end of the bar) observed pore diameter of the obtained porous tantalum vs. the applied potential (15 min anodization).

Table 3.1. NRA analysis

Time of anodization (min)	10	20	30	40	50	60
Oxide thickness (nm)	3.82	3.46	3.71	3.52	3.81	3.69
Relative error (nm)	0.08	0.076	0.079	0.077	0.080	0.078

I/t curves

Figure 3.3 shows the current density transient (chronoamperometry curve) recorded during anodization under a constant voltage of tantalum in "solution *A*". Such behavior is similar to that of the current density transient curves obtained on Al[23], Ti[24-27] when self organized pore formation took place. The shape of the i-t curve obtained at 18V can be divided into multiple stages associated with three different stages of pore formation. In the first stage (I), by a high-field mechanism[28], a compact layer of tantalum oxide is formed through hydrolysis of tantalum at the electrolyte-metal interface according to equation (1). This oxide layer leads to a dramatic decrease in the recorded current density due to it's poor electrical conductivity[8].

$$2Ta + 5\,H_2O \longrightarrow Ta_2O_5 + 10H^+ + 10e^- \qquad (1)$$

$$Ta_2O_5 + 14F^- + 10H^+ \longrightarrow 2TaF_7^{2-} + 5H_2O \qquad (2)$$

Due to the high solubility of the formed tantalum oxide in HF-containing solutions according to equation (2), pores start to grow and the current density increases gradually as the surface area increases. The origin of dissolving the tantalum oxide forming pores rather than uniform dissolution is not well known. At the beginning of stage (II) pores start to grow in a random manner where the degree of randomness depends on the electrochemical conditions. The pores continue to grow horizontally on the surface and the current consequently increases till the end point of stage (II) at which pores have the biggest possible diameter. At this point, the system starts to reach a steady state; stage (III), in which pore formation reaches equilibrium with pore dissolution.

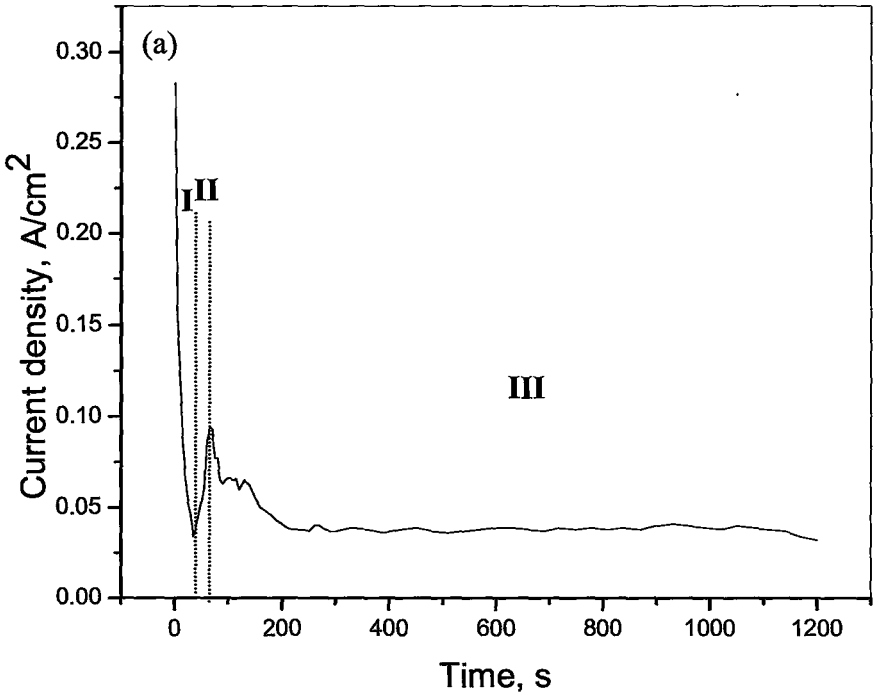

Figure 3.3. Chronoamperometric curve recorded while anodizing tantalum at 18V

The current density transients show different behavior when samples are anodized at different potentials. Figure 3.4 shows the i-t curves at 10, 12, 14 and 16V, in which stage II was not observed. The absence of stage II in the i-t obtained at 10V indicates the start of pore formation earlier at the first stage. Pore formation starts early because the applied anodizing potential was not high enough to make oxide film formation predominates at the first stage. This behavior noted at 10V starts to fade as the potential increases. At the i-t curve obtained at 12V, slight oscillations start to occur at stage II indicating a competition between the growing oxide and the pore formation (oxide dissolution). As the potential increases, at 14 and 16V, the oscillations become larger in amplitude and small peaks representing stage II are observed at 80 and 70 second for i-t curves of 14 and 16V respectively.

Fig. 5 shows the i-t curve at 20V at which a five times repetition of stage II (represented by the decaying five peaks) is observed at the first 135 seconds. It is believed that the occurrence of this kind of current oscillations is due to passivation and repassivation associated with the breakdown and healing of the oxide layer at relatively higher anodizing potentials. This oscillating behavior has been also reported for porous titanium oxide films[29].

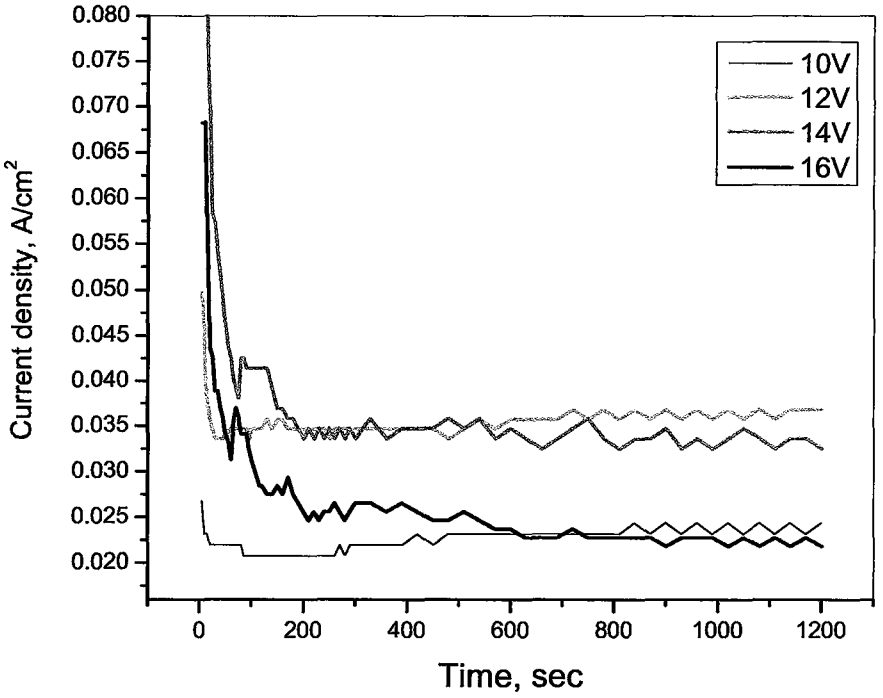

Figure 3.4. Chronoamperometric curves recorded while anodizing tantalum at 10, 12, 14 and 16V.

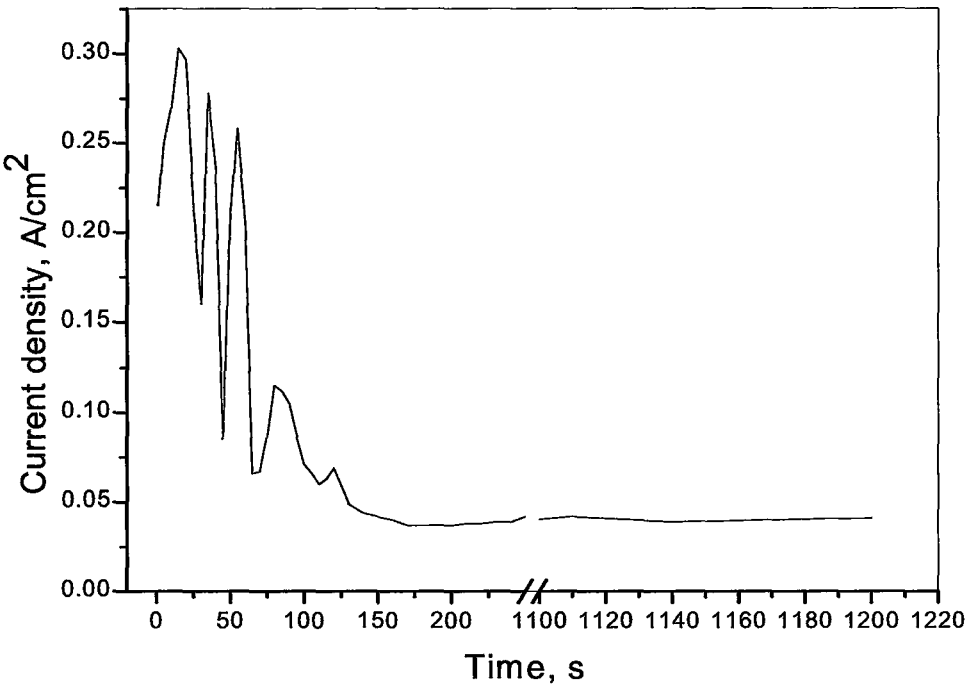

Figure 3.5. Chronoamperometric curve recorded while anodizing tantalum at 20V

When the chronoamperometric curves obtained in "solution *A*" are compared to the those obtained at dilute sulfuric acid solutions containing small quantities of HF (0.5-3%)[14], it can be observed that the current densities of the former are much higher than those of the later. These high values of current densities obtained in our study suggest a higher rate of tantalum oxide dissolution when a high concentrated sulfuric acid is used. Tantalum oxide films are known to consist of two layers, an inner layer of pure tantalum oxide next to the metal, and an outer layer of tantalum oxide that has some incorporated anions from the anodizing solution. The quantity of the anions incorporated in the outer layer depends on the concentration of the anodizing electrolyte. The nature and quantity of the incorporating anions affect the physical properties of the formed oxide film.

As early as 1954 Vermilyea[17] demonstrated a difference in chemical reactivity in HF between tantalum oxide films formed in concentrated and dilute sulfuric acid solutions[30]. The speed of chemical attack in HF solutions depends on the nature and concentration of the acid used for anodization. At 27.5°C it varies from 62±3 Å/min for tantalum oxide films formed in dilute sulfuric acid solutions, to about 500 Å/min for films formed in 95% H_2SO_4. In general, the films formed in concentrated solutions dissolve more rapidly than those formed in dilute solutions[28]. Therefore, it can be said that replacing dilute sulfuric acid, used in other studies to produce porous tantala, with concentrated sulfuric acid made a significant difference in the obtained porous structure. This simple change in the electrolyte made it possible to prepare the first metallic nanoporous tantalum by anodic oxidation.

3.5 Conclusion

A highly regular porous tantalum was fabricated by electrochemical oxidation of tantalum. The pore diameter could be controlled by changing applied anodizing voltage. The reported process can be used for synthesis of tantalum nanoporous templates for nanoparticles fabrication. The new template is compatible with the instant semiconductor industry and that may help incorporate it in applications of technological interest.

3.6 Acknowledgements

We acknowledge William N. Lennard (Interface Science Western) for his great assistance with the NRA analysis of our samples and Steve Koprich (Brockhouse Institute for Materials Research) for help with the SEM. We also thank Mark Greiner for his help with various aspects of this project and Gillian Goward (both McMaster) for helpful discussions. H. E. was supported by a post-graduate fellowship from the Ford Foundation (IFP program). Financial support was provided by the Department of Chemistry at McMaster University and the National Science and Engineering Research Council of Canada

3.7 References

1. Moriarty, P., Nanostructured materials. *Reports on Progress in Physics* **2001,** 64, (3), 297-381.
2. Huczko, A., Template-based synthesis of nanomaterials. *Applied Physics A-Materials Science & Processing* **2000,** 70, (4), 365-376.
3. Wade, T. L.; Wegrowe, J. E., Template synthesis of nanomaterials. *European Physical Journal-Applied Physics* **2005,** 29, (1), 3-22.
4. Chakarvarti, S. K.; Vetter, J., Template synthesis - A membrane based technology for generation of nano-/micro materials: A review. *Radiation Measurements* **1998,** 29, (2), 149-159.
5. Thompson, G. E., Porous anodic alumina: Fabrication, characterization and applications. *Thin Solid Films* **1997,** 297, (1-2), 192-201.
6. Masuda, H.; Fukuda, K., Ordered Metal Nanohole Arrays made by a 2-Step Replication of Honeycomb Structures of Anodic Alumina. *Science* **1995,** 268, (5216), 1466-1468.
7. Ghicov, A.; Tsuchiya, H.; Macak, J. M.; Schmuki, P., Titanium oxide nanotubes prepared in phosphate electrolytes. *Electrochemistry Communications* **2005,** 7, (5), 505-509.
8. Sieber, I.; Hildebrand, H.; Friedrich, A.; Schmuki, P., Formation of self-organized niobium porous oxide on niobium. *Electrochemistry Communications* **2005,** 7, (1), 97-100.

9. Tsuchiya, H.; Macak, J. M.; Sieber, I.; Taveira, L.; Ghicov, A.; Sirotna, K.; Schmuki, P., Self-organized porous WO_3 formed in NaF electrolytes. *Electrochemistry Communications* **2005,** 7, (3), 295-298.

10. Tsuchiya, H.; Macak, J. M.; Sieber, I.; Schmuki, P., Self-Organized High-Aspect-Ratio Nanoporous Zirconium Oxides Prepared by Electrochemical Anodization. *Small* **2005,** 1, (7), 722-725.

11. Sieber, I.; Kannan, B.; Schmuki, P., Self-assembled porous tantalum oxide prepared in H_2SO_4/HF electrolytes. *Electrochemical and Solid State Letters* **2005,** 8, (3), J10-J12.

12. Karlinsey, R. L., Preparation of self-organized niobium oxide microstructures via potentiostatic anodization. *Electrochemistry Communications* **2005,** 7, (12), 1190-1194.

13. Lu, Q.; Hashimoto, T.; Skeldon, P.; Thompson, G. E.; Habazaki, H.; Shimizu, K., Nanoporous anodic niobium oxide formed in phosphate/glycerol electrolyte. *Electrochemical and Solid State Letters* **2005,** 8, (5), B17-B20.

14. Sieber, I. V.; Schmuki, P., Porous tantalum oxide prepared by electrochemical anodic oxidation. *Journal of the Electrochemical Society* **2005,** 152, (9), C639-C644.

15. Sieber, I.; Hildebrand, H.; Friedrich, A.; Schmuki, P., Initiation of tantalum oxide pores grown on tantalum by potentiodynamic anodic oxidation. *Journal of Electroceramics* **2006,** 16, (1), 35-39.

16. Lu, Q.; Mato, S.; Skeldon, P.; Thompson, G. E.; Masheder, D.; Habazaki, H.; Shimizu, K., Anodic film growth on tantalum in dilute phosphoric acid solution at 20 and 85 degrees C. *Electrochimica Acta* **2002,** 47, (17), 2761-2767.

17. Vermilyea, D. A., Formation of anodic oxide films on tantalum in non-aqueous solutions. *Acta Met.* **1954,** 2, 483-486.

18. Shimizu, K.; Brown, G. M.; Habazaki, H.; Kobayashi, K.; Skeldon, P.; Thompson, G. E.; Wood, G. C., Direct observation of anodic films formed on tantalum in concentrated phosphoric and sulphuric acid solutions. *Corrosion Science* **1998,** 40, (6), 963-973.

19. Davies, J. A.; Norton, P. R., Absolute coverage measurement of adsorbed carbon monoxide and molecular deuterium on platinum. *Nuclear Instruments & Methods* **1980,** 168, (1-3), 611-615.

20. Asoh, H.; Nishio, K.; Nakao, M.; Tamamura, T.; Masuda, H., Conditions for fabrication of ideally ordered anodic porous alumina using pretextured Al. *Journal of the Electrochemical Society* **2001,** 148, (4), B152-B156.

21. Kerrec, O.; Devilliers, D.; Groult, H.; Chemla, M., Dielectric properties of anodic oxide films on tantalum. *Electrochimica Acta* **1995,** 40, 719-724.

22. Macagno, V.; Schultze, J. W., The growth and properties of thin oxide layers on tantalum electrodes. *Journal of Electroanalytical Chemistry* **1984,** 180, (1-2), 157-170.

23. Parkhutik, V. P.; Shershulsky, V. I., Theoretical Modeling of Porous Oxide-Growth on Aluminum. *Journal of Physics D-Applied Physics* **1992,** 25, (8), 1258-1263.

24. Beranek, R.; Hildebrand, H.; Schmuki, P., Self-organized porous titanium oxide prepared in H_2SO_4/HF electrolytes. *Electrochemical and Solid State Letters* **2003,** 6, (3), B12-B14.

25. Gong, D.; Grimes, C. A.; Varghese, O. K.; Hu, W. C.; Singh, R. S.; Chen, Z.; Dickey, E. C., Titanium oxide nanotube arrays prepared by anodic oxidation. *Journal of Materials Research* **2001,** 16, (12), 3331-3334.

26. Zwilling, V.; Darque-Ceretti, E.; Boutry-Forveille, A.; David, D.; Perrin, M. Y.; Aucouturier, M., Structure and physicochemistry of anodic oxide films on titanium and TA6V alloy. *Surface and Interface Analysis* **1999,** 27, (7), 629-637.

27. Cai, Q. Y.; Paulose, M.; Varghese, O. K.; Grimes, C. A., The effect of electrolyte composition on the fabrication of self-organized titanium oxide nanotube arrays by anodic oxidation. *Journal of Materials Research* **2005,** 20, (1), 230-236.

28. Young, L., Anodic Oxide Films. **1961**, 377.

29. Yu, X. F.; Li, Y. X.; Ge, W. Y.; Yang, Q. B.; Zhu, N. F.; Kalantar-Zadeh, K., Formation of nanoporous titanium oxide films on silicon substrates using an anodization process. *Nanotechnology* **2006,** 17, (3), 808-814.

30. Amsel, G.; Cherki, C.; Feuillade, G.; Nadai, J. P., Influence of the electrolyte on the composition of 'anodic oxide films' on tantalum. *Journal of Physics and Chemistry of Solids* **1969,** 30, (9), 2117-2134.

CHAPTER 4

Highly ordered porous tantalum, a new nanotemplate prepared by anodic oxidation

H. ElSayed, S. Singh, and P. Kruse

4.1 Abstract:

In this paper we study the electrochemical conditions that may affect porous tantalum formation. The highly ordered porous tantalum (HOPT) that we have previously reported for the first time was found to be affected by some electrochemical conditions such as solution aging and anodization potential. As a possible new template for nanofabrication, reproducibility of (HOPT) is very crucial. We have found that porous tantalum can be reproducibly prepared within the anodization potential range 10-20 V. Monodispersity of pore diameters was found to be the highest when 15 V is used for the anodic oxidation. The new template may find several potential technological applications for being made of metal that is already compatible with the semiconductor industry.

4.2 Introduction

The scientific and technological importance of porous materials comes from their large surface area and ordered structure[1]. The International Union of Pure and Applied Chemistry (IUPAC) classifies porous materials into three categories; micropores of less than 2 nm in diameter, mesopores between 2 and 50 nm, and macropores of greater than 50 n^2. In general, nanoporous materials are defined as porous materials with pore diameter less than 100 nm.

While nanoporous materials are widely used as adsorbents, catalyst support, and membrane materials, there is a great demand for the use of high quality monodisperse nanoporous materials in a diversity of applications, such as high density storage media, chemical sensors of high sensitivity, nano-electronic devices, functional biochemical membranes and the fabrication of catalytic nanoparticles[3].

The classical deposition of nanoparticles from solution is characterized by relatively poor particle size homogeneity and spatial particle distribution[4]. Other nanofabrication strategies have been used such as optical lithography. Creating sub-100 nm structures using optical lithography techniques, however, has been challenging and will require extensive equipment upgrades to employ short-wavelength light sources and optics[5]. Lithographic techniques, such as focused ion beam (FIB) milling , electron-beam lithography (EBL), and scanning probe microscopy (SPM) as direct write methods are capable of writing only small areas (hundreds of square micrometers) and they have low throughput[6].

In conclusion, each of the aforementioned techniques has its own advantages and disadvantages, and challenges that can slow down nanofabrication progress can be summarized in the following: (i) expensive equipments, (ii) time consuming processes, (iii) impracticality with mass production, (iv) inadequate control over shape and size of nanostructures, and (v) inability to pattern large areas in short times[5].

The ability to assemble nanoparticles into arrays, networks and circuits in an accurate and controlled manner and the same time having a control over their shape and size represents an important key to fabricate variety of nanodevices. Networks of metallic or semiconducting nanoparticles, or quantum dots, may find potential applications as nanometre scale sensors, advanced computer architectures, ultra-dense memories and quantum-information processing[7]. One of the simple and easy to do methods recently demonstrated successful control over size and shape of nanoparticles is the template-assisted nanofabrication[8, 9]. This method involves the synthesis of the desired nanostructures inside the pores of the nanoporous membrane. Porous anodic alumina (PAA) is the most studied nanoporous membrane for nanostructure fabrication[1].

The growth of PAA on aluminum under anodic polarization in various electrolytes began in the mid-1900s when Keller[10] et al. reported details on cell structure and anodic voltage dependence of the cell size[3], where a cell is the unit area containing a single nanohole, as they defined it. Anodically oxidized alumina film consists of nanoholes that grow normal to the surface. Later several authors[11-13] discussed the mechanism of nanohole formation by electrical field assisted dissolution. Recently Masuda et al.[14, 15] reported self-organized pore growth, leading to a densely packed hexagonal pore structure

for certain sets of parameters PAA has been widely used as a template for preparing nanostructures with a wide range of materials[3, 16]. PAA has not been employed technologically because of the fragile nature of alumina, for example, PAA can not be used in semiconductor industry because it does not resist mechanical stresses.

Seeking for a new nanofabrication template that has enhanced properties, other metals such as Ti[17], Sn[18], Zr[19], Nb[20], W[21] and Ta[22-24] have been electrochemically treated to investigate the formation of self-organized pores. Anodic oxidation of Titanium in phosphate electrolytes containing small amounts of fluoride ions resulted in self-ordered titanium oxide nanotubes[25]. On the other hand, irregular porous oxide films were obtained by anodic oxidation of niobium[20, 26, 27], and tungsten[21]. Recently, randomly distributed pores of tantalum oxide with a wide pore distribution were obtained by electrochemical oxidation of tantalum in dilute sulfuric acid solutions containing small quantities of HF (0.5-3%)[22-24].

In this paper we investigate in more depth the electrochemical conditions that can affect the formation of porous tantalum developed in our lab. We have previously reported the fabrication of 2D highly ordered porous tantalum[28] that can be used as a nanofabrication template. The porous tantalum was prepared by direct and simple electrochemical anodization of tantalum in a mixture of a concentrated sulfuric acid and a dilute HF solution. The template has shown pore diameter tunability in the range 25-55 nm with changing the applied anodization potential. The compatibility of tantalum with present semiconductor industry makes the new template a candidate for potential technological applications.

4.3 Experimental work

Materials and surface preparation

Prior to anodization, tantalum foil (Alfaaesar, 99.95%, 0.127 mm) was rinsed in acetone, isopropanol, and Millipore water (18.2 MΩ/cm resistively). No polishing process was adapted. Anodization was carried out in a stirred solution of concentrated H_2SO_4 (95-98%) and HF (48%) in a volume ratio 9:1. (This solution will be referred to below as "solution *A*.") The solutions were prepared from reagent-grade chemicals and Millipore water.

Electrochemical experiments

Anodization was conducted using a conventional two-electrode system connected to a power supply (Agilent E3615A). A Pt/Ir wire was used as the counter-electrode (cathode). The working electrode (anode) was tantalum foil substrate connected with a copper wire to the power supply. The distance between the working and counter-electrodes was kept at 1.5 cm. During anodization, solution was stirred using a magnetic bar. All the experiments were performed at room temperature (approximately 20°C). Immediately after anodization, the sample was rinsed with deionized water.

Scanning electron microscopy and Atomic force microscopy surface investigations

The surface view of the anodized samples were acquired on a field emission scanning electron microscope (FE-SEM Jeol 7000F). The AFM used is Digital Instruments Nanoscope III system, a Multimode SPM.

Nuclear reaction analysis (NRA) measurements

The $^{16}O(d,p)^{17}O$ nuclear reaction was used to determine the absolute oxygen content of the anodized samples within ~0.5 μm of the surface. The $^{16}O(d,p)^{17}O$ reaction used an 972 KeV deuterium beam as the primary beam. The incident beam is approximately $1mm^2$ in area. The ion beam was incident on the samples along the surface normal and the detector was placed at 125° in the scattering plane which included the incident beam. The tantalum oxide thickness was estimated by comparing the number of protons emitted from the sample to those emitted from a reference Ta_2O_5 sample of known oxygen coverage and oxide thickness using the $^{16}O(d, p)^{17}O$ reaction. The accuracy of this measurement is about ±5% if the sample and reference have similar geometry. More about the experimental setup of the NRA system can be found elsewhere[29].

4.4 Results and Discussion:

In our previous study[28] we demonstrated for the first time the formation of highly ordered porous tantalum (HOPT) by anodic oxidation. In this paper we show in more details the reproducibility of HOPT at different electrochemical conditions of anodization potential and anodizing time. We also show that large domains of pores can be obtained on the tantalum surface. Table 1 shows different electrochemical conditions of anodization potential and anodization time at which porous tantalum was prepared.

Sample number	Anodization potential, V	Anodizing time, min
1(a)	15	10
1(b)	20	45
1(c)	20	15
1(d)	12	10
1(e)	12	20
1(f)	20	15

Table 4.1. Different electrochemical etching parameters used for porous tantalum fabrication by anodization of tantalum in "solution *A*".

The field emission scanning electron microscope (FE-SEM) images 1a, 1b, and 1c show the large domains of pores successfully prepared in different etching conditions (see table 1). Figure 4.1 shows the top view of porous tantalum samples prepared at different electrochemical etching parameters mentioned in table 1.

In FESEM image 1(a) the pore diameters show a very high degree of monodispersity, where the average diameter is ~ 30 nm. Anodization of tantalum in "solution *A*" to obtain highly ordered pores was found to be reproducible in the voltage range 10-20 V and anodizing time 5-60 minutes, anodization times longer than one hour have not been investigated. show surface view of porous tantalum samples by FE-SEM. Images 1(b) and 1(c) show large domains (a few square micrometers) of pores of high monodisperse diameters.

Although porous tantalum samples 1(d) and 1(e), grown at same potential (12V), were subjected to different anodizing times (10 and 20 minutes), their corresponding FESEM images show pores of average diameter in the range 27-29 nm confirming the high reproducibility of the pores and the independent of pore diameter on anodizing time. Image 1(f) shows an FE-SEM images of porous tantalum grown at 20 V for 15 minute anodizing time. The sample shows that bigger pores can be obtained by applying higher values of potential. The pores obtained in this specific sample have diameters in the range 35-55 nm. It is also clear from the image that the pores are arranges in close packed hexagonal structures, where every pore is surrounded by six neighboring pores.

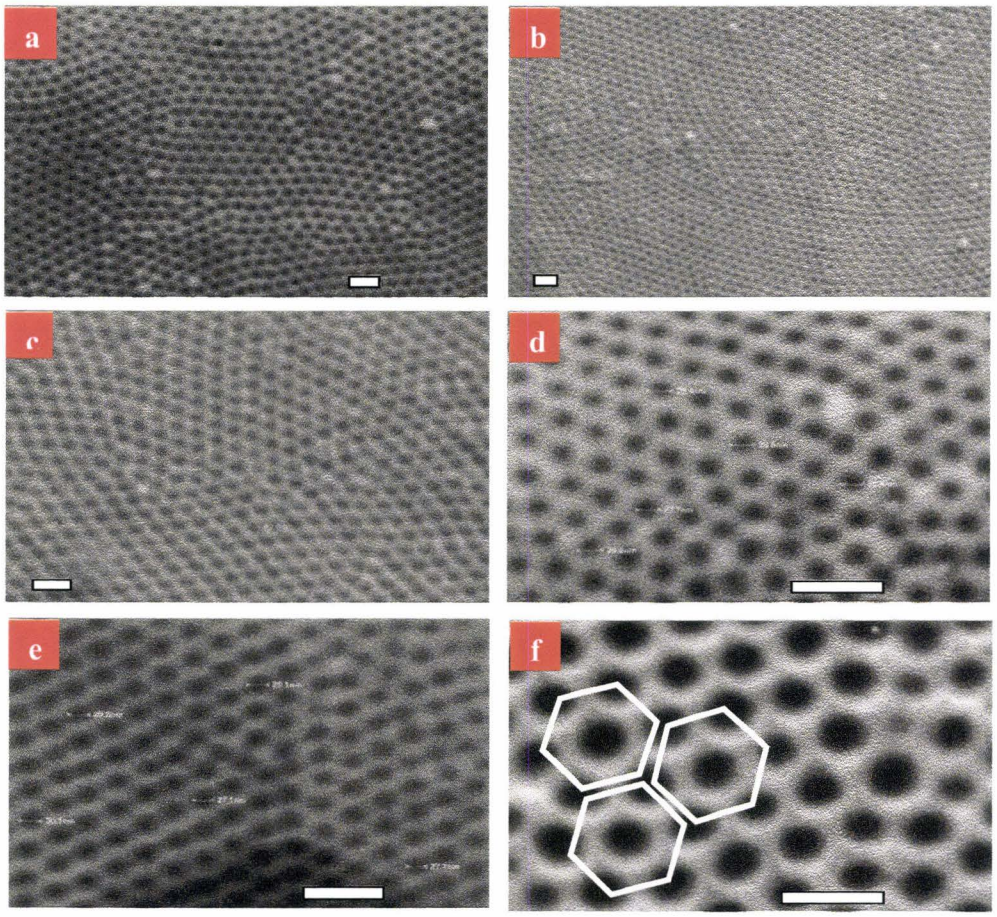

Figure 4.1. SEM images of porous tantalum. a, anodized for 10 min at 15V. **b**, anodized for 10 min at 12V. **c**, anodized for 20 min at 12V. **d**, anodized for 15 min at 20V. e, anodized for 20 min at 12 V. and f, anodized for 15 min at 20 V. (*All the rod bars are 100 nm*)

Figure 4.2 shows the pore diameter and diameter monodispersity with respect to anodization potential. This graph was obtained by anodizing tantalum samples for 15 minutes each at potentials 10, 12, 14, 15, 16, 18, and 20V. The minimum and maximum observed pore diameter, at each potential, of the obtained porous tantalum were graphed versus the applied potential. The graph not only shows the dependence of pore diameter on anodizing potential, in which there is a trend of pore diameter increase as the applied potential increases, but it also illustrates that highest monodisperse porous tantalum is obtained at anodization potential of 15 V.

When applying anodizing potential less or higher than 15 V, highly ordered pores are obtained but of low monodispersity. For instance, pores of diameters in the range 35-50 nm are obtained when anodizing potential of 20 v is applied, and when a potential of 10 V is applied, pores of diameters in the range 22-28 nm are obtained. When several tantalum samples were anodized for different times of anodization and at 15 V, they all show pores of diameters in the range 27-29 nm regardless the anodizing time.

In the previous studies on pore formation of other valve metals such as Ti[1], anodizing period and the applied anodizing potential strongly affected the surface morphology of the formed oxide film. Therefore, in order to investigate the influence of applied potential on the morphology of the resulting porous tantalum, a set of experiments were performed at potentials higher than 20 V, and field emission scanning electron microscope (FE-SEM) micrographs of the anodized thin films were taken and observed. SEM micrographs showed that porous tantalum oxide was formed and the quality of the porosity depends on the applied anodizing potential.

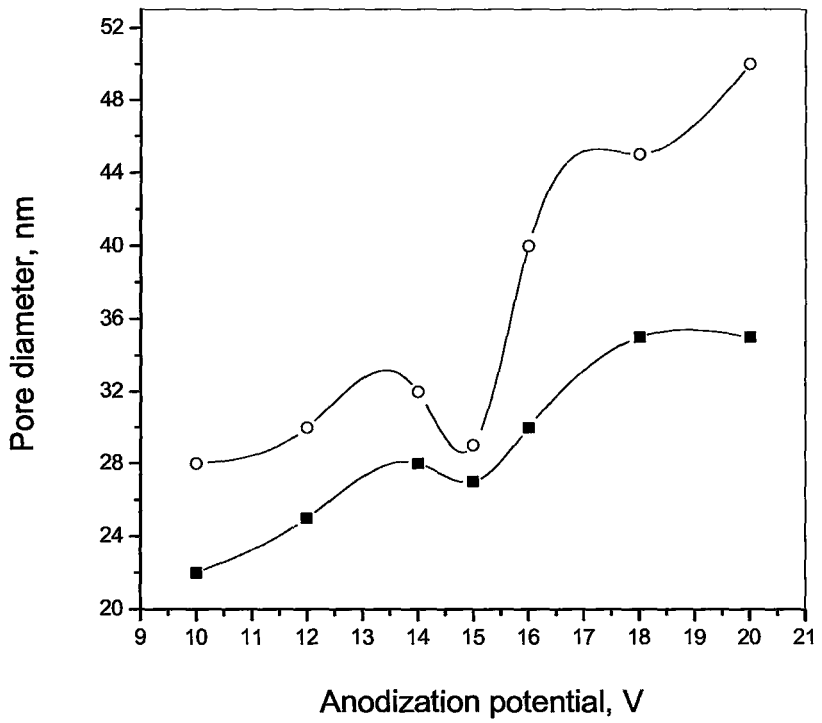

Figure 4.2. Pore diameter and diameter monodispersity with respect to anodization potential. The minimum (lower curve) and maximum (higher curve) observed pore diameter of the obtained porous tantalum vs. the applied potential (15 min anodization).

Figure 4.3 shows SEM micrographs taken for a tantalum sample after anodization at 40V for 20 minutes. The relatively high applied potential not only cause surface deformation, but also it caused differential etching. SEM Images 4.3(b), (c) and (d) represents three images for three different grains labeled i, ii, and iii on image 3a. It is very clear from the images that no highly ordered pores were formed and the surface morphology of the different grains are completely different after the electrochemical etching. Figure 4.3(b) shows porous granules in which the average pore diameter is in the range 10-30 nm. Figure 4.3(c) shows a different surface morphology in which no pores were observed and only granules 50-100 nm big were uniformly distributed on the surface except at some spots. At these spots, circled in the image, no granules were observed and only valleys 100-120 nm big were observed. Image 3d shows a porous surface in which the valleys observed in image 4c was repeated on almost the whole surface of the grain. The observed surface morphological features suggest a differential etching against "solution *A*" as a result of different etching resistance shown by different tantalum grains.

One possible explanation for such behavior is that when anodizing at relatively high potentials, the rate of field-enhanced dissolution is much faster than that of the formation of the nanopores.

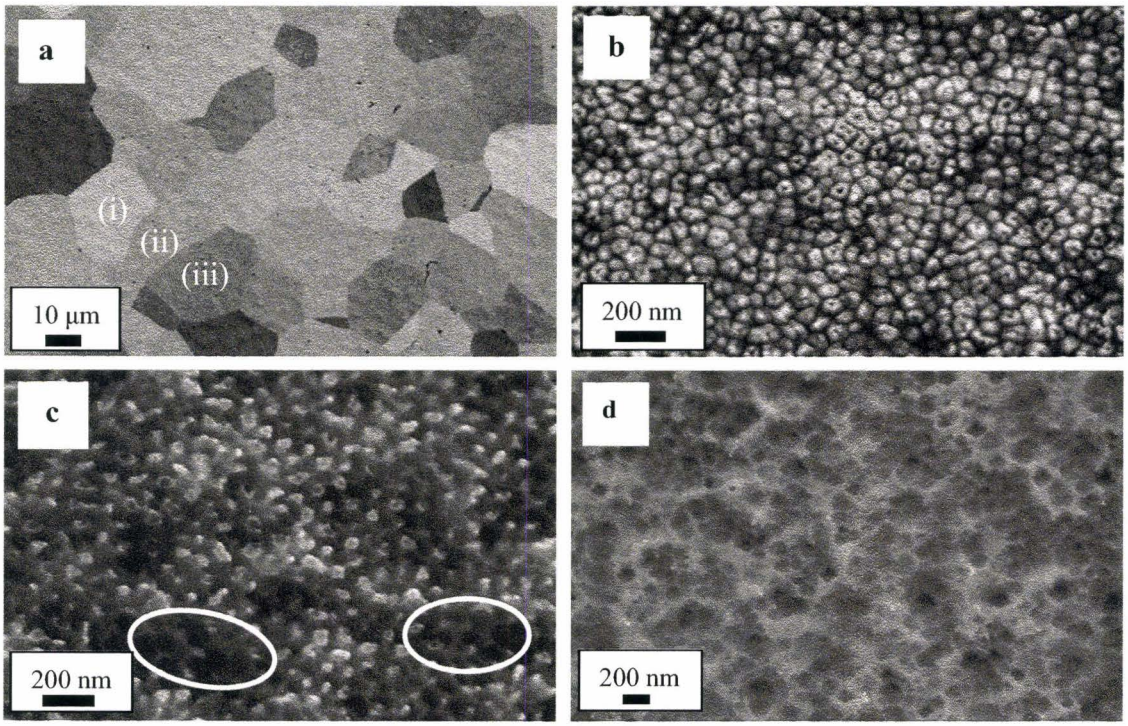

Figure 4.3. SEM micrographs for a tantalum sample after anodization at 40V for 20 minutes.

The mechanism of pore formation has been investigated by chronoamperometry in our previous study on porous tantalum[28]. Figure 4.4 shows the chronoamperometric (i-t) curve obtained for the anodization of tantalum in "solution *A*" at 18 V. The shape of the curve can be divided into three phases associated with three different stages of pore formation. In the first phase (I), a compact layer of tantalum oxide is formed, by a high-field mechanism[30], through tantalum hydrolysis at the electrolyte-metal interface according to equation (1). The formed oxide layer is characterized by poor electrical conductivity[30] that leads to a dramatic decrease in the recorded current density.

$$2Ta + 5\,H_2O \longrightarrow Ta_2O_5 + 10H^+ + 10e^- \quad (1)$$

$$Ta_2O_5 + 14F^- + 10H^+ \longrightarrow 2TaF_7^{2-} + 5H_2O \quad (2)$$

At the second phase (II), pores start to form and grow due to the high solubility of the formed tantalum oxide film in HF-containing solutions according to equation (2). This dissolution of tantalum oxide film appears as a gradual increase in the current density. The current density continues increasing, as result of growing pores on the surface, till the end point of phase (II) at which pores have the biggest possible diameter. The system starts to reach a steady state when pore formation reaches equilibrium with pore dissolution; phase (III).

In our previous study[28] we have shown that the chronoamperometric curves obtained at constant potentials (10 – 20 V), where pores are formed, show slightly different behaviors depending on the applied anodizing voltage. The differences observed

between these curves occur mainly in the early stages (0 – 200 s) of anodization, but they all reach steady state condition in less than 400 s. It was found that the steady state current density reached for each curve depends on the applied potential. Figure 4.5 shows the relation between the applied anodizing potential and the corresponding steady state current obtained from the chronoamperometric curves[28]. Overall, steady state current density increases linearly with increasing the applied potential. This can be attributed to the increase in the rate of field-enhanced dissolution of the formed tantalum oxide, as fluoride-complexes, over that of oxide formation as potential increases.

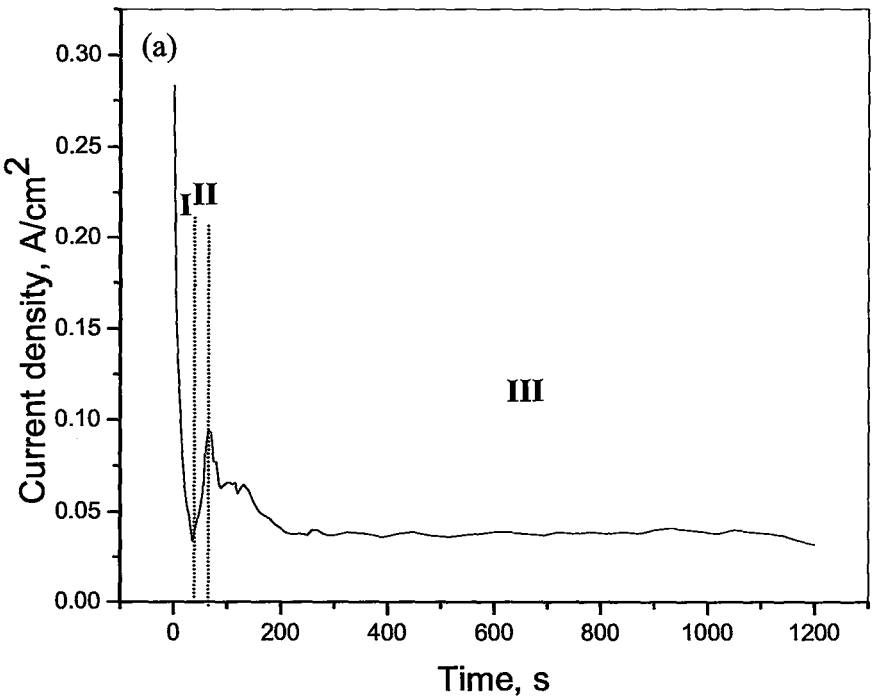

Figure 4.4. Chronoamperometric curve recorded while anodizing tantalum at 18 V

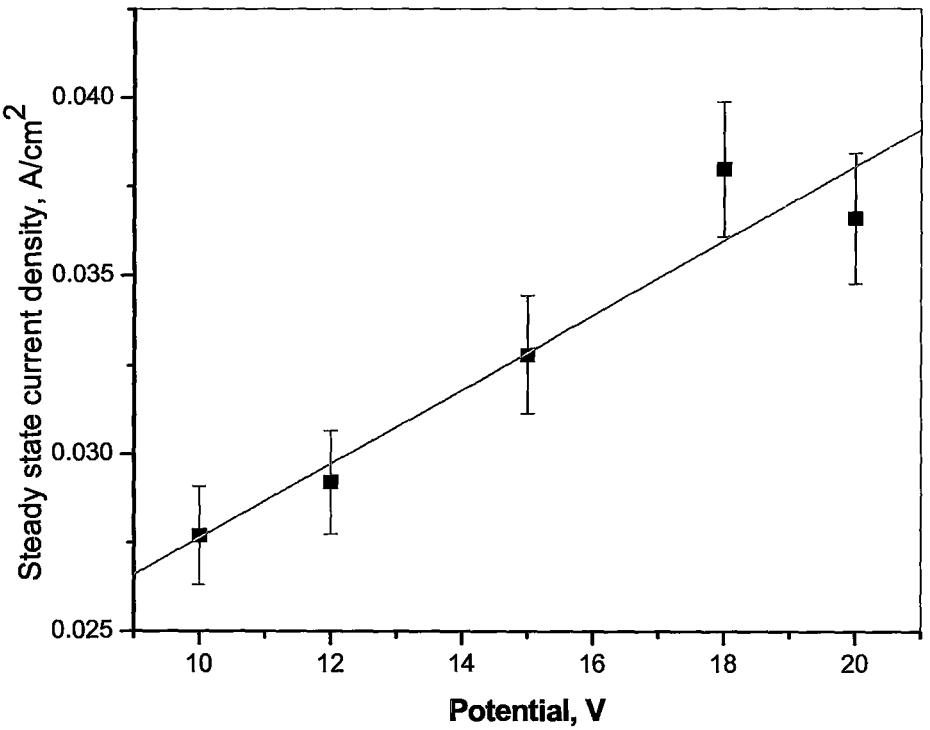

Figure 4.5. Steady state current density for tantalum during the electrochemical anodization in "solution *A*".

The oxide thickness on top of porous tantalum was estimated by Nuclear reaction Analysis (NRA). NRA gives the total number of oxygen atoms in a given sample surface area and compare it to that of a flat tantalum oxide thin film of known thickness, thus tantalum oxide thickness on porous tantalum can be estimated by comparison. Using NRA, the absolute thicknesses of tantalum oxide films on porous tantalum samples grown at different anodizing times were found to be close to the value of native tantalum oxide thickness. All the thickness estimated are in the range 3.0-3.7 nm, and the native tantalum oxide thickness is known from the literature to be 1-2nm[31, 32]. The overestimation of tantalum oxide thickness is due to the incorporation of electrolyte anions (SO_4^{2-}) into the oxide film during the anodization process. It is known that sulphate anions can be incorporated into the whole depth of the film when the oxide is grown in highly concentrated sulfuric acid (95-98%)[33].

The NRA data also shows that the oxide thickness does not depend on time of anodization. This finding is different than that reported by Schmoki et al group[23, 24], in which they have shown that the thickness of the porous tantalum oxide increases with anodization time when dilute sulfuric acid is used as etching electrolyte. The reason of forming porous tantalum rather than porous tantala can be attributed to using concentrated sulfuric acid in the etching electrolyte. In 1954 Vermilyea[34] reported a difference in chemical reactivity in HF between tantalum oxide films formed in concentrated and dilute sulfuric acid solutions. This difference in chemical reactivity towards HF solutions and in chemical and physical properties in general is attributed to the incorporation of electrolyte anions into the oxide film. The incorporation is not effective when dilute acids are used

for anodization. Tantalum oxide films formed in concentrated solutions were found to dissolve more rapidly than those formed in dilute solutions[35]. Thus most of the tantalum oxide formed by anodic oxidation is susceptible to dissolution in HF solution.

Tantalum oxide films dissolve in the etching solution as tantalum fluoride complex (TaF_7^{2-}). The effect of soluble tantalum fluoride on the morphology and pore formation was studied. It was found that the high ordering of pores resulting from tantalum oxide dissolution is affected by the age of the solution. Figure 4.6 shows FE-SEM images of three porous tantalum samples (a, b, and c) anodized for 10 minutes at 15 V. Sample (a) was anodized in 10 ml of "solution *A*" containing 0.17 g of Ta as tantalum fluoride complex (0.093 M Ta^{+4}), sample (b) was anodized in 10 ml of "solution *A*" containing 0.26 g of Ta (0.143 M), and sample (c) was anodized under the same conditions in a solution containing 0.29 g of Ta (0.16 M). It can be observed from the images that the roughness of the porous tantalum surface increases as the concentration of tantalum ions increases. The pores were obtained in the three samples but the defects increases and the quality of pore ordering decreases as the tantalum ion concentration increases in the solution.

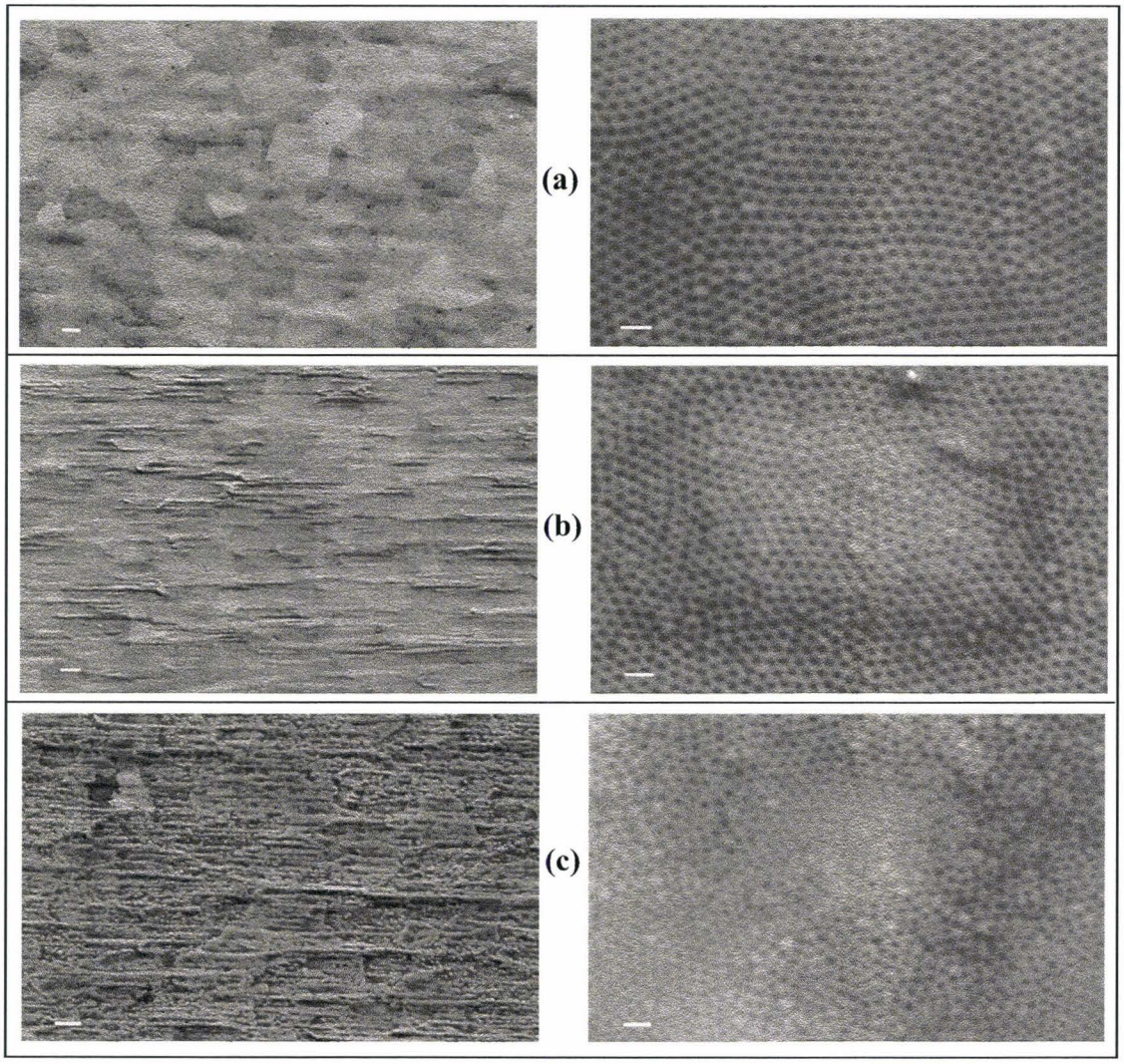

Figure 4.6. Effect of soluble tantalum fluoride on the morphology and pore formation.

4.5 Conclusion

Highly regular porous tantalum can be obtained by electrochemical oxidation of tantalum in a mixture of concentrated sulfuric acid and dilute hydrofluoric acid. The pore diameter, that can be controlled by the applied anodizing potential, shows high reproducibility. The rang of potential that can be applied to produce pores is 10-20 V and the best anodizing potential to produce monodisperse, highly symmetric, and well ordered pores is 15 V. Aging of the etching solution affects the morphology of the obtained porous tantalum, and pores can be even obtained using a solution as aged as a solution containing 0.143 M Ta^{4+}. The reported process can be used for synthesis of tantalum nanoporous templates for nanoparticles fabrication. The new template is compatible with the instant semiconductor industry and that may help incorporate it in applications of technological interest.

4.6 Acknowledgements

We acknowledge William N. Lennard (Interface Science Western) for his great assistance with the NRA analysis of our samples and Steve Koprich (Brockhouse Institute for Materials Research) for help with the SEM. We also thank Mark Greiner for his help with various aspects of this project and Gillian Goward (both McMaster) for helpful discussions. H. E. was supported by a post-graduate fellowship from the Ford Foundation (IFP program). Financial support was provided by the Department of Chemistry at McMaster University and the National Science and Engineering Research Council of Canada.

References

1. Yu, X. F.; Li, Y. X.; Ge, W. Y.; Yang, Q. B.; Zhu, N. F.; Kalantar-Zadeh, K., Formation of nanoporous titanium oxide films on silicon substrates using an anodization process. *Nanotechnology* **2006,** 17, (3), 808-814.
2. Lu, G. Q.; Zhao, X. S., *Nanoporous materials : science and engineering.* first ed.; Imperial College Press: London, 2005; 'Vol.' 4, p 912.
3. Shingubara, S., Fabrication of nanomaterials using porous alumina templates. *Journal of Nanoparticle Research* **2003,** 5, (1-2), 17-30.
4. Ueda, M.; Dietz, H.; Anders, A.; Kneppe, H.; Meixner, A.; Plieth, W., Double-pulse technique as an electrochemical tool for controlling the preparation of metallic nanoparticles. *Electrochimica Acta* **2002,** 48, (4), 377-386.
5. Henzie, J.; Barton, J. E.; Stender, C. L.; Odom, T. W., Large-area nanoscale patterning: Chemistry meets fabrication. *Accounts of Chemical Research* **2006,** 39, (4), 249-257.
6. Gates, B. D.; Xu, Q. B.; Stewart, M.; Ryan, D.; Willson, C. G.; Whitesides, G. M., New approaches to nanofabrication: Molding, printing, and other techniques. *Chemical reviews* **2005,** 105, (4), 1171-1196.
7. Mendes, P. M.; Chen, Y.; Palmer, R. E.; Nikitin, K.; Fitzmaurice, D.; Preece, J. A., Nanostructures from nanoparticles. *Journal of Physics-Condensed Matter* **2003,** 15, (42), S3047-S3063.
8. Huczko, A., Template-based synthesis of nanomaterials. *Applied Physics A-Materials Science & Processing* **2000,** 70, (4), 365-376.

9. Wade, T. L.; Wegrowe, J. E., Template synthesis of nanomaterials. *European Physical Journal-Applied Physics* **2005,** 29, (1), 3-22.

10. Keller, F.; Hunter, M. S.; Robinson, D. L., Structural features of oxide coatings on aluminum. **1953,** 100, 411.

11. Hoar, T. P.; Mott, N. F., A mechanism for the formation of porous anodic oxide films on aluminium. **1959,** 9, 97.

12. O'Sullivan, J. P.; Wood, G. C., Nucleation and growth of porous anodic films on aluminum. **1970,** A317, 511.

13. Thompson, G. E.; Furneaux, R. C.; Wood, G. C.; Richardson, J. A.; Goode, J. S., Nucleation and growth of porous anodic films on aluminum. **1978,** 272, 433.

14. Masuda, H.; Fukuda, K., Ordered Metal Nanohole Arrays made by a 2-Step Replication of Honeycomb Structures of Anodic Alumina. *Science* **1995,** 268, (5216), 1466-1468.

15. Masuda, H.; Hasegwa, F.; Ono, S., Self-ordering of cell arrangement of anodic porous alumina formed in sulfuric acid solution. *Journal of the Electrochemical Society* **1997,** 144, (5), L127-L130.

16. Xia, Z.; Riester, L.; Sheldon, B. W.; Curtin, W. A.; Liang, J.; Yin, A.; Xu, J. M., Mechanical properties of highly ordered nanoporous anodic alumina membranes. *Reviews on Advanced Materials Science* **2004,** 6, (2), 131-139.

17. Macak, J. M.; Tsuchiya, H.; Taveira, L.; Aldabergerova, S.; Schmuki, P., Smooth Anodic TiO_2 Nanotubes. *Angewandte Chemie International Edition* **2005,** 44, (45), 7463-7465.

18. Shin, H. C.; Dong, J.; Liu, M. L., Porous tin oxides prepared using an anodic oxidation process. *Advanced Materials* **2004,** 16, (3), 237.

19. Tsuchiya, H.; Macak, J. e.; M.; Sieber, I.; Schmuki, P., Self-Organized High-Aspect-Ratio Nanoporous Zirconium Oxides Prepared by Electrochemical Anodization. *Small* **2005,** 1, (7), 722-725.

20. Lu, Q.; Hashimoto, T.; Skeldon, P.; Thompson, G. E.; Habazaki, H.; Shimizu, K., Nanoporous anodic niobium oxide formed in phosphate/glycerol electrolyte. *Electrochemical and Solid State Letters* **2005,** 8, (5), B17-B20.

21. Tsuchiya, H.; Macak, J. M.; Sieber, I.; Taveira, L.; Ghicov, A.; Sirotna, K.; Schmuki, P., Self-organized porous WO_3 formed in NaF electrolytes. *Electrochemistry Communications* **2005,** 7, (3), 295-298.

22. Sieber, I.; Hildebrand, H.; Friedrich, A.; Schmuki, P., Initiation of tantalum oxide pores grown on tantalum by potentiodynamic anodic oxidation. *Journal of Electroceramics* **2006,** 16, (1), 35-39.

23. Sieber, I.; Kannan, B.; Schmuki, P., Self-assembled porous tantalum oxide prepared in H_2SO_4/HF electrolytes. *Electrochemical and Solid State Letters* **2005,** 8, (3), J10-J12.

24. Sieber, I. V.; Schmuki, P., Porous tantalum oxide prepared by electrochemical anodic oxidation. *Journal of the Electrochemical Society* **2005,** 152, (9), C639-C644.

25. Ghicov, A.; Tsuchiya, H.; Macak, J. M.; Schmuki, P., Titanium oxide nanotubes prepared in phosphate electrolytes. *Electrochemistry Communications* **2005,** 7, (5), 505-509.

26. Karlinsey, R. L., Preparation of self-organized niobium oxide microstructures via potentiostatic anodization. *Electrochemistry Communications* **2005,** 7, (12), 1190-1194.

27. Sieber, I.; Hildebrand, H.; Friedrich, A.; Schmuki, P., Formation of self-organized niobium porous oxide on niobium. *Electrochemistry Communications* **2005,** 7, (1), 97-100.

28. Chapter 3.

29. Davies, J. A.; Norton, P. R., Absolute coverage measurement of adsorbed carbon monoxide and molecular deuterium on platinum. *Section Title: Surface Chemistry and Colloids. Nuclear Instruments & Methods* **1980,** 168, (1-3), 611-615.

30. Young, L., Anodic Oxide Films. *Section Title: Electrochemistry* **1961**, 377.

31. Kerrec, O.; Devilliers, D.; Groult, H.; Chemla, M., Dielectric properties of anodic oxide films on tantalum. *Electrochimica Acta* **1995,** 40, 719-724.

32. Macagno, V.; Schultze, J. W., The growth and properties of thin oxide layers on tantalum electrodes. *Journal of Electroanalytical Chemistry* **1984,** 180, (1-2), 157-170.

33. Shimizu, K.; Brown, G. M.; Habazaki, H.; Kobayashi, K.; Skeldon, P.; Thompson, G. E.; Wood, G. C., Direct observation of anodic films formed on

tantalum in concentrated phosphoric and sulphuric acid solutions. *Corrosion Science* **1998,** 40, (6), 963-973.

34. Vermilyea, D. A., Formation of anodic oxide films on tantalum in non-aqueous solutions. *Acta Met.* **1954,** 2, 483-486.

35. Amsel, G.; Cherki, C.; Feuillade, G.; Nadai, J. P., Influence of the electrolyte on the composition of 'anodic oxide films' on tantalum. *Journal of Physics and Chemistry of Solids* **1969,** 30, (9), 2117-2134.

CHAPTER5

Conclusion

Electrochemical patterning of tantalum was achieved using two strategies; selective electrodeposition, and electrochemical etching. In the first method copper was selectively deposited on pre-patterned tantalum oxide thin films based on an electrical behavior of tantalum oxide thin films in which they are semiconducting for thicknesses less than 15 nm, and insulating for thicknesses beyond 15 nm. They also form Schottky junctions when certain metals such as Cu are deposited on them. Utilizing this behaviour, tantalum substrates with areas of relatively thick tantalum oxide films (>20 nm) and thin tantalum oxide films (~4-5 nm) made by a sharp tungsten tip scratching were selectively electroplated with copper. Copper was deposited only in the opening made by the tip where the tantalum oxide is the thinnest. Cyclic voltammetry studies have confirmed the electrical nature of that copper Ta_2O_5 (~4-5 nm)/Cu interface to be a Schottky contact. A high quality Schottky interface between the copper lines and the substrate is beneficial to applications such as four probe measurements of nanoscale objects (e. g. carbon nanotubes), where conduction through the bulk must be excluded. In this study, copper has shown poor nucleation when electrodeposited on tantalum oxide thin films and that in turn was reflected on the nature of deposited copper lines. The deposited lines suffered discontinuity and that may be a challenge of using copper is this process. In the next step of this project, selective electroplating of other metals of technological importance such as gold, and silver on pre-patterned Ta_2O_5 thin films may be investigated seeking for the best system in which fine and continuous metal lines or arbitrary shapes can be obtained.

Further electrical characterization can be performed on the selectively deposited lines by obtaining current-voltage characteristics of the dry system to confirm the presence of Schottky junction at the metal/ tantalum oxide interface.

The second approach of tantalum nanopatterning lead to the discovery of highly ordered nanoporous tantalum. Recently, anodization of tantalum in sulfuric/HF electrolyte has been shown to produce randomly distributed pores. In our study, tantalum was electrochemically etched in an appropriate electrolyte to form highly ordered nanoporous tantalum. The new discovery can be used as a template for nanoparticles fabrication, as it has symmetric pores of potential dependent tunable character. The template that has the highest hardness among other porous metals and can resist mechanical stresses is already compatible with the present semiconductor industry, thus it is a good candidate to be employed in many potential technological applications. The system we have discovered still needs more investigations. If it is used as a template for nanoparticles fabrication, it is worth finding the electrochemical parameters at which smaller or deeper pores, higher pore diameter monodispersity can be obtained. In general, the system needs to be extensively studied to make it a universal template for nanofabrication.